ELSEVIER

Biophysical Chemistry 117 (2005) 173 – 190

Biophysical Chemistry

http://www.elsevier.com/locate/biophyschem

Analysis of the modal hypothesis of Ca^{2+}-dependent inactivation of L-type Ca^{2+} channels

Nick I. Markevich[a,b,*], Oleg Y. Pimenov[a], Yury M. Kokoz[a]

[a]*Institute of Theoretical and Experimental Biophysics, Russian Academy of Sciences, Pushchino, Moscow 142290, Russia*
[b]*Department of Pathology, Anatomy and Cell Biology, Thomas Jefferson University, Room 233, JAH, 1020 Locust St., Philadelphia, PA 19107, USA*

Received 25 April 2005; received in revised form 28 April 2005; accepted 28 April 2005
Available online 4 June 2005

Abstract

A kinetic model of Ca^{2+}-dependent inactivation (CDI) of L-type Ca^{2+} channels was developed. The model is based on the hypothesis that postulates the existence of four short-lived modes with lifetimes of a few hundreds of milliseconds. Our findings suggest that the transitions between the modes is primarily determined by the binding of Ca^{2+} to two intracellular allosteric sites located in different motifs of the CI region, which have greatly differing binding rates for Ca^{2+} (different k_{on}). The slow-binding site is controlled by local Ca^{2+} near a single open channel that is consistent with the "domain" CDI model, and Ca^{2+} binding to the fast-binding site(s) depends on Ca^{2+} arising from distant sources that is consistent with the "shell" CDI model. The model helps to explain numerous experimental findings that are poorly understood so far.
© 2005 Elsevier B.V. All rights reserved.

Keywords: Ca^{2+}-dependent inactivation; Gating mode; Mathematical model

1. Introduction

High-threshold voltage-dependent L-type Ca^{2+} channels play a key role in the contraction of smooth and cardiac muscles, neuroendocrine secretion, and many other vital functions of the organisms. They are regulated by a great number of factors of different physicochemical nature [1,2]. Among the most important are hormones and neurotransmitters, which bring about a relatively slow regulation (up to a few tens of seconds), and membrane potential (V) and intracellular calcium, which accomplish a fast regulation (of the order of hundreds of milliseconds). The slow regulation is mainly related to chemical modification, including (de)phosphorylation of channels, which is associated with cascades of enzymes whose activity is modulated by hormones and neurotransmitters [1]. The fast regulation is determined by voltage- and Ca^{2+}-dependent conformational transitions in the channel.

The L-type Ca^{2+} current that develops in response to membrane depolarization can be divided into the following components: voltage-dependent activation, Ca^{2+}-dependent inactivation (CDI), voltage-dependent inactivation (VDI), and residual current [1,3]. The inactivation of the channel with time t is usually described by the double-exponential function $I(t)=A_{Ca}\cdot\exp(-t/\tau_{Ca})+A_V\cdot\exp(-t/\tau_V)+I_0$, where A_{Ca} and A_V are the amplitudes, τ_{Ca} and τ_V are the time constants of CDI and VDI, respectively, and I_0 is the residual current. Despite the simple kinetics of the L-type Ca^{2+} current and abundant experimental evidence that has accumulated over a period of more than 25 years, both the molecular and kinetic mechanisms of regulation of the current are not yet completely understood to explain the dependencies of amplitudes and time constants of different inactivation components on V and intracellular Ca^{2+} concentration.

In the last decade, considerable progress has been made towards understanding the molecular mechanism of CDI.

* Corresponding author. Department of Pathology, Anatomy and Cell Biology, Thomas Jefferson University, Room 233, JAH, 1020 Locust St., Philadelphia, PA 19107, USA. Tel.: +1 215 503 4794; fax: +1 215 923 2218.
E-mail address: Nikolai.Markevitch@jefferson.edu (N.I. Markevich).

0301-4622/$ - see front matter © 2005 Elsevier B.V. All rights reserved.
doi:10.1016/j.bpc.2005.04.017

The critical determinants of Ca^{2+} inactivation have been localized in the C-terminal tail (residues 1520–1732) of the pore-forming α_1-subunit of L-type Ca^{2+} channel [4,5] referred to as the Ca^{2+} inactivation (CI) region [6]. It was shown that replacing the CI region with the homologous segment of the Ca^{2+}-insensitive α_{1E}-subunit of Ca^{2+} channel results in a complete suppression of CDI [4]. Further experiments with the substitution or deletion of amino acid sequences and individual amino acids in the CI region [6–14] made it possible to identify several narrow regions responsible for CDI, the most important of which are the consensus EF hand motif, a region designated peptide LM1 [11] or peptide A [12], and the IQ-like motif. It was shown that the binding of Ca^{2+} to the peptide A and IQ-like regions occurs via calmodulin (CaM) [6,10,12–17].

Despite significant advances in the localization of sites responsible for CDI and proposed molecular mechanisms for CDI [15,18], there is only one report [11] using recent molecular experimental data in which an attempt was made to analyze quantitatively the sequence of transitions of the channels from one state to another. As before, a lot of the experimental data on the kinetics of L-type Ca^{2+} currents in native membranes, obtained over a period of more than two decades, remain unexplained. A quantitative description of the L-type Ca^{2+} currents in rat ventricular myocytes [19] is rather phenomenological.

One of the difficulties in interpreting the experimental data is that the kinetics of CDI is largely affected not only by conformational changes in the channel but also by changes in intracellular Ca^{2+} concentration near the membrane, which significantly vary near open and closed channels. To explain the dependence of CDI kinetics on Ca^{2+} arising from both local and distant sources [20], the analysis of CDI must take into account a highly variable distribution of intracellular Ca^{2+} along the inner membrane surface.

The most popular models of CDI of L-type channels, which account for changes in Ca^{2+} concentration near the membrane, are the shell [21] and the domain [22] models. The shell model postulates that inactivation is driven by Ca^{2+}, which is uniformly distributed in a thin layer (up to 1 μm) adjacent to the intracellular membrane surface. The concentration of Ca^{2+} in this layer is determined by the whole-cell integral Ca^{2+} current and the intracellular Ca^{2+} buffer [21]. The transition of the channel into the inactivated state occurs when Ca^{2+} binds to the allosteric sites of both the open and closed channels. By contrast, the domain model assumes that the transition to the inactivated state occurs if local Ca^{2+} binds to the allosteric site of the open channel only [22]. Both models have some shortcomings, which were discussed in the literature [22,23]. Thus, the shell model cannot explain the experimentally observed CDI in single channels, while the domain model ignores the role of the concentration of Ca^{2+} near closed channels, that is Ca^{2+} arising by lateral diffusion from distant open channels, and consequently does not account for the experimentally observed effect of intracellular Ca^{2+}-binding buffer on the kinetics of channel inactivation [21]. In view of this, the development of a general kinetic model of CDI, which could explain a wide variety of experimental data on the kinetics of integral and gating currents and on single channels is an important task.

The finding that voltage- and Ca^{2+}-dependent transitions of L-type channels are independent processes significantly contributed to understanding the mechanism of intrachannel conformational changes leading to the CDI of channels. The analysis indicated that the movement of activating [24] and inactivating gating currents [25,26] does not depend on intracellular Ca^{2+} concentration. This was an essential premise to the modal hypothesis of Ca^{2+}-dependent inactivation of Ca^{2+} channels proposed by Imredy and Yue [27]. The hypothesis is based on the assumption that intracellular calcium both induces inactivation and causes the channel to adopt a new conformation characterized by another mode of openings and closings of the channel, namely, mode M_{Ca}. The M_{Ca} mode is characterized by a larger first latency [27,28]. Based on this, the authors proposed a kinetic model of CDI with two modes (basal mode, M_1, and M_{Ca}) in which brief transitions of gating are solely determined by voltage. However, the authors restricted themselves to a detailed description of the stationary kinetics of channel opening in both modes and did not analyze possible mechanisms of Ca^{2+}-dependent transitions. The dependence of the kinetic characteristics of L-type current on intracellular Ca^{2+} concentration was not investigated.

In this study, we propose a refined kinetic model, which accounts more accurately for the CDI of L-type channel at both the whole-cell and single-channel levels. The model is based on the hypothesis that postulates the existence of four short-lived modes with lifetimes of a few hundreds of milliseconds. Our findings suggest that the transitions between the modes is primarily determined by the binding of Ca^{2+} to two intracellular allosteric sites located in different motifs of the CI region, which have greatly differing binding rates for Ca^{2+} (different k_{on}). The slow-binding site is controlled by local Ca^{2+} near a single open channel, and Ca^{2+} binding to the fast-binding site(s) depends on Ca^{2+} arising from distant sources.

2. Model development

2.1. A kinetic scheme of voltage-dependent transitions in one mode

2.1.1. Voltage-dependent activation

There is substantial evidences that four most extracellularly located basic residues of the S4 segment of the α_1 subunit serve as the voltage sensors for activation of the Ca^{2+} channel [29,30]. These sensors move outward and

rotate at membrane depolarization, initiating a conformational change that opens the channel. The simplest and most widely accepted kinetic model of voltage-dependent activation of Ca^{2+} channels is a scheme with two closed (C_1 and C_2) and one open (O) states [31,32]:

$$C_1 \underset{k_{-1}}{\overset{k_{+1}}{\Leftrightarrow}} C_2 \underset{k_{-2}}{\overset{k_{+2}}{\Leftrightarrow}} O \quad (1)$$

According to this scheme, only the rate constants k_{+1} and k_{-1} of step 1 are voltage-dependent, and the rate constants k_{+2} and k_{-2} are weakly dependent on voltage. The existence of two short-lived closed states is supported by the biexponential dependence of the closed time distribution in the mllisecond range [32,33]. Surely, the assumption of two closed states is oversimplified. The number of closed states may be much greater; it may be even infinitely large, as proposed by Shirokov et al. [34] who described the kinetics of channel opening and inactivation using equations of electrodiffusion. However, based on the above data, one can say with a fair degree of confidence that there are two high potential barriers to the transition of the channel from the first closed state to the open state, i.e., there are two stable closed states.

The assumption that the second step (opening) is voltage-independent is supported by data showing that the duration of the channel open state is independent of potential [35,36]. There are some objections against this scheme [33], which are based on the fact that tail currents arising during membrane repolarization are very fast. In reality, they are limited by the rate of voltage clamp. Therefore, it is assumed that the potential-independent closing of the channel cannot account for the rapid deactivation at hyperpolarizing voltages. In addition, there is evidence that the open state duration depends on potential [37]. At first sight, the conflicting data on the voltage dependence of the open channel duration can be reconciled by assuming that, at voltages above −30 mV, the open channel duration depends weakly on voltage, and a strong dependence on V is observed only at more negative potentials. If so, then there should exist an activation gating charge associated with the $C_2 \Leftrightarrow O$ transition. This gating charge is distributed according to the Boltzman equation in a strongly negative range of potentials and has a time constant of a few milliseconds. However, a detailed analysis of gating currents in the range of potentials up to −150 mV [25,26] shows the absence of the gating currents associated with the activation of Ca^{2+} channels. In addition, if both activation steps were voltage-dependent, there would be a strong difference in the slope (K) of the Boltzman distribution with respect to the value of the gating charge and channel conductance (the open probability). However, simultaneous measurements of integral and gating currents in cardiocytes [38] demonstrate approximately equal slopes for both characteristics ($K \approx 11$ mV). Therefore, in what follows, only the $C_1 \Leftrightarrow C_2$ transition is taken to be potential-dependent. The discrepancy in the experimental data on the voltage dependence of the open channel duration in this case can be explained by the existence of several open states in different modes, which are in a voltage-dependent equilibrium.

2.1.2. Voltage-dependent inactivation

VDI of L-type Ca^{2+} channels is actually a complex process [39–41], which may consist of several different Ca^{2+}-independent components with a duration from about 10 ms [42] to a few seconds [43], depending on conditions. For instance, the VDI of native cardiac L-type channels shows fast ($\tau_f \sim 30$ ms) and slow ($\tau_s \sim 300$ ms) components related to the phosphorylation of channels [41]. The molecular determinants of VDI have been intensively studied and appear to be located in the transmembrane segments S6 in repeats I–IV [42] and I–II linker [40] of the α_1 subunit and also include the β subunit [44] of the L-type Ca^{2+} channel. In this paper, we will follow the classical view according to which VDI is a slow component of I_{CaL}.

The most important feature of VDI of L-type Ca^{2+} channels is the presence of two inactivated states and a gating charge that determines the transition between these states [25,26]. This gating charge was detected and characterized by Shirokov et al. [25,26] and named charge 2 to differentiate it from activating charge 1. Charge 2 has the same valence as charge 1 but is distributed according to the Boltzman equation in the range of more negative potentials (potential of half-activation, V, ≈ -90 mV) and has a time constant of ≈10 ms. It was suggested that the following kinetic model of interconversions of charges 1 and 2 [26]

$$\begin{array}{ccc} I_1 & \Leftrightarrow^{\text{charge 2}} & I_2 \\ \Updownarrow & & \Updownarrow \\ C & \Leftrightarrow_{\text{charge 1}} & O \end{array} \quad (2)$$

Here C, O, I_1 and I_2 are the closed, open, and inactivated states, respectively. The transfer of the activating gating charge 1 occurs during the $C \Leftrightarrow O$ transition, and charge 2 is transferred during the $I_1 \Leftrightarrow I_2$ transition. The voltage-independent stage $O \Leftrightarrow I_2$ determines the time constant of VDI of the L-type Ca^{2+} current.

2.1.3. A general scheme of voltage-dependent switches of L-type Ca^{2+} currents within one mode

Based on the schemes of activation (1) and inactivation (2), the following schemes of voltage-dependent switches of the Ca^{2+} channel within active, M_B and M_F (Fig. 1A), and inactive, M_I and M_{Ca} (Fig. 1B), modes were proposed (see also Fig. 2). In inactive modes in Fig. 1B, an inactivated state I_3 was introduced instead of the open state O in Fig. 1A. Stages $C_1 \Leftrightarrow C_2$ and $I_1 \Leftrightarrow I_2$ are voltage-dependent. The other steps, including transition $C_2 \Leftrightarrow I_3$, are independent on voltage. It should be noted that the scheme in Fig. 1A is

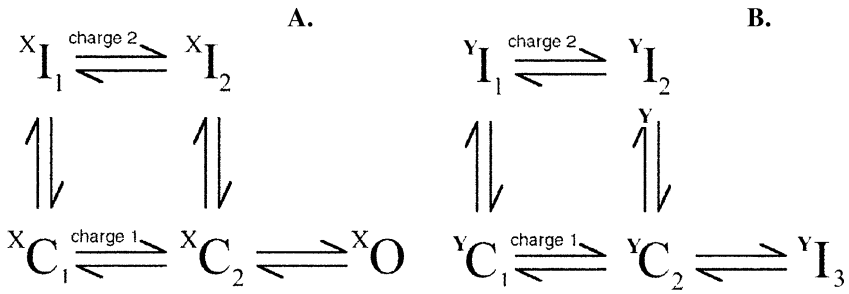

Fig. 1. Voltage-dependent transitions in active (A) and inactive (B) modes. Every gating mode comprises five states labeled by superscripts X (X=B, F) or Y (Y=I, Ca). C_1 and C_2 are closed, I_1 and I_2 are voltage-dependent inactivated, I_3 is Ca^{2+}-dependent inactivated, and O is open states of the channel, respectively. X denotes active, basal (M_B) and flickering (M_F), modes. States in inactive, intermediate (M_I) and calcium (M_{Ca}) modes are labeled by superscripts Y. For detailed mode description, see Fig. 2 and text.

analogous to the scheme of voltage-dependent switches of T-type Ca^{2+} channels suggested by Chen and Hess [45]. According to this scheme, the transition to the inactivated state I_2 occurs from the closed state C_2. In principle, an alternative scheme is also possible in which the transition to I_2 occurs from the open state O [45]. However, there is evidence that the transition of L-type Ca^{2+} channels to the inactivated state during membrane depolarization occurs from the closed state [46]. Therefore, in further analysis, we will use the kinetic schemes in Fig. 1A and B as the basic models of channel voltage-dependent switches within the active mode M_X (X=B, F) and the inactive mode M_Y (Y=I, Ca), respectively (all modes will be described below). A detailed scheme of all intramodal transitions is given in Appendix A.

2.2. A kinetic scheme of Ca^{2+}-dependent transitions between different modes

The simplest scheme of Ca^{2+}-dependent transitions of channels from one mode to another is the scheme of Imredy and Yue [27], which involves two conformations corresponding to two modes of Ca^{2+}-dependent inactivation of L-type Ca^{2+} channels, the basal mode M_1 and the calcium-dependent mode M_{Ca}.

$$M_1 \overset{Ca^{2+}}{\Leftrightarrow} M_{Ca} \quad (3)$$

According to this scheme, intracellular Ca^{2+} binds to the channel (the mechanism of binding is not specified) and induces a transition from the active mode M_1 to the inactive Ca^{2+}-dependent mode M_{Ca}. Openings and closings of the channel in each mode are described by identical kinetic schemes with two closed and one open states (scheme 1). In order that the condition of independence of the activation gating current from the intracellular Ca^{2+} concentration is met, it is assumed that the rate constants of the potential-dependent C1 ⇔ C2 transition in both modes are equal. The main difference between the modes is the decrease in the rate constant of the entry of channels into the open state (k_{+2} in Scheme (1)). It was assumed that, upon transition to M_{Ca}, k_{+2} decreases by two orders of magnitude and becomes equal to $\approx 0.005\ ms^{-1}$. The rate constant (k_{-2}) for the exit from the open state increases only slightly. Using this hypothesis, the authors explained their own experimental data on two-pulse stimulation of single channels, in particular, a substantial decrease in the time of the first opening of the channel after its preliminary stimulation by membrane potential, i.e., after the transition to M_{Ca}.

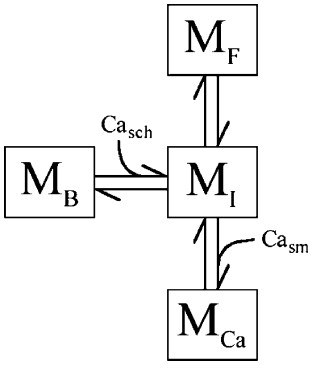

Fig. 2. A scheme of intermodal Ca^{2+}-dependent transitions in L-type Ca^{2+} channels. M_B, M_I, M_F, M_{Ca} denote the basal active, intermediate inactive, flickering active, and calcium inactive modes of the channel. Ca_{sch} (subchannel) and Ca_{sm} (submembrane) are the intracellular calcium concentrations near the mouths of the open and closed channels, respectively.

However, this simple scheme of intermodal switches (3) does not completely describe the reported experimental data. Indeed, if the channel is in M_{Ca} ($k_{+2} \approx 0.005\ ms^{-1}$), the time of the first opening will be very long (more than 100 ms), which agrees well with the data of the authors. However, after the first opening, the channel closes, and more than 100 ms are needed in order that the channel reopens. Consequently, the channel in M_{Ca} is able to generate only rare single openings with a period of about 100 ms. This pattern of openings is observed in experiments and is conventionally called the active mode 0_a. However, in the experiments of Imredy and Yue, the first opening of the channel, which occurs with a long latency, is almost always followed by frequent openings and closings in the form of short pulse bursts [27]. Similar, though more rare, pulse bursts in single channels are also observed at very high Ca^{2+} concentrations of up to tens of micromolar [28]. Therefore,

it is reasonable to suggest that the delayed first opening of the channel upon repeated membrane depolarization results from a slow transition from inactive mode M_{Ca} to a second active mode rather than from a slow entry into the open state. The occurrence of one more active mode (to which the channel transits during membrane depolarization) is indirectly supported by abundant experimental data on residual currents through L-type Ca^{2+} channels. Below this mode will be referred to as the flickering mode (M_F), by analogy with the term "flickering state" introduced by Mazzanti et al. [37] to describe residual currents. Taking this into account, we propose the following modification of the kinetic model of intermodal transitions, which, in addition to three above-cited modes, mode M_1 (the basal mode M_B), mode M_{Ca}, and mode M_F includes an inactive intermediate mode M_I (Fig. 2).

M_B denotes the basal active mode, which is an analogue of the M_1 mode in the model of Imredy and Yue [27]; Ca_{sch} (subchannel) and Ca_{sm} (submembrane) are the intracellular calcium concentrations near the mouths of the open and closed channels, respectively. Our preliminary analysis indicated that the model involving only three modes, M_B, M_{Ca}, and M_F, is inconsistent with the experimental data. Thus, it predicts a proportional change in the amplitudes of peak and residual currents upon variations of intracellular Ca^{2+} concentration, whereas in the experiments, a strong change in the residual current is observed at a virtually invariant amplitude of the peak current in the presence of the Ca^{2+}-binding buffer [21,47]. Based on this, we suggested that there are four modes of which two modes, M_B and M_F, are active, and modes M_{Ca} and M_I are inactive.

The model postulates that the channel has two, a fast and a slow, allosteric sites for Ca^{2+} binding with different association constants k_{on}, which are responsible for CDI. The binding of Ca^{2+} to the allosteric sites occurs in a strict order. Initially, immediately after the channel opening in the M_B mode, Ca^{2+} binds only to the slow site having a very low association constant for Ca^{2+}($k_{on}^{slow} \approx 10^6$ M^{-1} s^{-1}). The second allosteric site with a high association constant is not accessible for Ca^{2+} binding. As a result, the channel switches from M_B to the intermediate mode M_I.

Very low values k_{on}^{slow} are required to explain the gradual dependence of the time constant (τ_{Ca}) of CDI on very high local Ca^{2+} concentration Ca_{sch} which is determined by the value of the single channel current [48–51]. Only after the transition to the inactive mode M_I, the second site(s) with a high affinity for Ca^{2+}($K_{d2} \approx 10^{-7}$–10^{-6} M) becomes exposed and the second calcium ion binds to them. In this case, the channel switches from M_I to M_{Ca}. A high-affinity allosteric site is required to explain the dependence of CDI on submembrane Ca^{2+} concentration Ca_{sm} (10^{-7}–10^{-6} M) near closed channels and in Ca^{2+}-binding buffer. If the second calcium ion does not bind to the second allosteric site, the channel can spontaneously switch from M_I to M_F. It is assumed that transitions from M_I to M_{Ca} occur in two steps: the first step is Ca^{2+}-dependent, and the second step does not depend on intracellular Ca^{2+}. That is, the channel first transits from M_I to M_{Ca1} after the calcium ion binds to the site having a high affinity for Ca^{2+}, and then the channel spontaneously transits from M_{Ca1} to M_{Ca2}. The Ca^{2+}-independent step in the transition from M_I to M_{Ca} is necessary to explain the saturation effect in the inactivation of Ca^{2+} channels by very high (tens of micromolar) Ca^{2+} concentrations [28]. A detailed scheme of all intermodal transitions is given in Appendix A.

The schemes of voltage- and Ca^{2+}-dependent transitions presented in Figs. 1 and 2 completely describe the proposed kinetic model of VDI and CDI in L-type Ca^{2+} channels. In order that the condition of independence of activating and inactivating gating currents on intracellular Ca^{2+} concentration is met, it is proposed that all the modes have identical kinetic parameters of the voltage-dependent steps. Thus, the modes differ from each other only by voltage-independent steps. Besides, channels in inactive modes, M_I and M_{Ca}, may exist in the Ca^{2+}-induced inactivated state, I_3, as distinct from active modes M_B and M_F in which channels may be in the open state O (Fig. 1). The absence of the open state in the intermediate mode M_I is of fundamental importance. This postulate derives from the assumption that the transition from M_I to M_{Ca} is regulated only by intracellular Ca^{2+} arising from distant sources, i.e., Ca^{2+} near closed channel, Ca_{sm}, whose concentration is not very high (up to a few micromolar) and is determined by the integral Ca^{2+} current through the membrane and by the Ca^{2+}-binding buffer. This Ca^{2+} inactivation step has features typical of CDI in the shell model [21]. Although the possibility exists that channels in M_{Ca} can be open [27], we assumed for simplicity that all channels in mode M_{Ca} are closed.

Besides, it is proposed that not only Ca^{2+} at the mouth of open channels (Ca_{sch}) is involved in the regulation of the transition from M_B to M_I. The switches of channels in closed states (C_1 and C_2) between these modes are also regulated by Ca^{2+} concentration near closed channels (Ca_{sm}). It is very important that the dissociation constant for Ca^{2+} binding in all states, open and closed, is the same to keep independence of gating currents on the intracellular Ca^{2+} concentration [24]. These switches are presented in a detailed scheme of intermodal transitions (Appendix A). However, since local Ca_{sch} is incomparably higher than Ca_{sm}, the entry of the channel into CDI after the depolarization-induced activation of the channel is regulated only by Ca_{sch}, as it is shown in Fig. 2. The regulation of CDI by local Ca^{2+} is consistent with the domain model of CDI [22] in which Ca^{2+} binds only to the open channel. The involvement of Ca_{sm} in the regulation of transitions of channels in closed states between these modes is crucial when the channel exits from the CDI induced by membrane hyperpolarization.

According to the model, the charge transfer in the membrane occurs only during $C_1 \Leftrightarrow C_2$ and $I_1 \Leftrightarrow I_2$ transitions; therefore, the rate constants $k_{C1,C2}$, $k_{C2,C1}$, $k_{I1,I2}$, and

$k_{I2,I1}$ depend on membrane potential. The dependence of these constants on membrane potential is given by the following expressions [26]:

$$k_{C_1,C_2} = \alpha_1 \exp\left(\frac{(V-V_1)}{2K} - 0.1\left(\frac{(V-V_1)}{2K}\right)^2\right)$$

$$k_{C_2,C_1} = \alpha_1 \exp\left(\frac{(V_1-V)}{2K} - 0.1\left(\frac{(V-V_1)}{2K}\right)^2\right)$$

$$k_{I_1,I_2} = \alpha_2 \exp\left(\frac{(V-V_2)}{2K} - 0.1\left(\frac{(V-V_2)}{2K}\right)^2\right)$$

$$k_{I_2,I_1} = \alpha_2 \exp\left(\frac{(V_2-V)}{2K} - 0.1\left(\frac{(V-V_2)}{2K}\right)^2\right). \quad (4)$$

Here K characterizes the slope of the voltage dependence of the gating charge being transferred (if the valencies of the activation [z_1] and inactivation [z_2] charges are equal and are approximately $z_1=z_2=z$, then $K=RT/Fz$). V_1 and V_2 are the potentials at which half the maximum gating charge is transferred; α_1 and α_2 are the rate constants at $V=V_1$ and $V=V_2$, respectively.

2.3. Some molecular aspects of CDI of L-type Ca^{2+} channels

Recent experimental studies revealed the molecular determinants for CDI [5–15] and made it possible to localize the regions of the channel that correspond to the allosteric sites. A very attractive candidate for the first allosteric site sensitive to very high local Ca_{sch} could be the consensus EF hand motif [5] which has a low affinity (10–50 μM) for Ca^{2+} [52]. CaM is not involved in the binding of intracellular Ca^{2+} to this site. If it was the case, the second site regulated by Ca_{sm} arising from distant open Ca^{2+} channels would be located on CaM tethered to the IQ-like motif [6,10,13–16] or/and CaM tethered to the CI region designated peptide LM1 [12] or peptide A [13].

However, the experimental data [11,53,54] do not support that hypothesis. Yue et al. [5,11] were the first to suggest that the consensus EF hand motif of the α_{1C} subunit (EF hand) is the critical molecular determinant for CDI. First, using their own experimental data, they proposed that the EF hand was a Ca^{2+} sensor for CDI [5]. However, a detailed analysis of mutations in the Ca^{2+}-coordinating center of the EF hand showed that the mutations have a modest influence on CDI [11,53,54]. Therefore, Peterson et al. [11] reconsidered the hypothesis that the EF hand serves as a contributory Ca^{2+} inactivation sensor and suggested a kinetic model based on the hypothesis that the EF hand may only support the transduction of Ca^{2+}-CaM binding into channel inactivation. According to the hypothesis of Peterson et al. [11], Ca^{2+} binds only to CaM tethered to the IQ-like region, and only after the binding of Ca^{2+}, a conformational change in the EF region takes place, which supports CDI.

Following the hypothesis of Peterson et al. [11], we may propose that the first allosteric site, which is regulated by local Ca_{sch}, is located on CaM tethered to the IQ-like motif. However, in this case the following paradox arises [11]. How can high-affinity Ca^{2+} binding to CaM (the submicromolar range) [55] be gradually regulated by very high concentrations of local Ca_{sch} (submillimolar range)?

There are several possible explanations for the unsaturated binding of Ca_{sch} to CaM to induce CDI. The simplest explanation proposed in our model is a very slow binding of Ca^{2+} to the first allosteric site:

$$O - CaM + Ca \underset{k_{-1}}{\overset{k_1}{\Leftrightarrow}} I - CaM - Ca \quad (5)$$

where O-CaM and I-CaM are the complexes of CaM with the IQ motif in open and inactivated conformations of the channel.

It is suggested that the association constant (k_1) of Ca^{2+} binding to CaM tethered to the IQ motif is very low ($k_1 \cdot [Ca_{sch}] < 0.1$ ms^{-1} or $k_1 < 10^6$ M^{-1} s^{-1} (10^{-3} μM^{-1} ms^{-1}) at $Ca_{sch} \sim 100$ μM) to explain the dependence of the time constant (τ_{Ca}) of CDI on single channel current, which determines Ca_{sch} [48–51]. Another possibility suggested by Peterson et al. [11] is that slow binding of Ca^{2+} to CaM is followed by fast Ca^{2+}-independent inactivation of the channel:

$$O - CaM + Ca \underset{k_{-1}}{\overset{k_1}{\Leftrightarrow}} O - CaM - Ca \underset{k_{-2}}{\overset{k_2}{\Leftrightarrow}} I - CaM - Ca \quad (6)$$

where O-CaM-Ca is the open state of the channel.

In this case, the slow first step determines τ_{Ca}. It should be noted that, with very fast Ca^{2+}-independent second step, this scheme turns to scheme (5). The experimental data show accelerated Ba^{2+} inactivation at different mutations in the IQ region [8,13–15,56] and support that hypothesis about the fast Ca^{2+}-independent transition following Ca^{2+} binding to CaM. Moreover, it was shown [42] that the time constant of the fast Ca^{2+}-independent component of inactivation may be as low as 10 ms.

Another reason for the gradual regulation of τ_{Ca} by local Ca_{sch} could be the dependence of the apparent dissociation constant for Ca^{2+}/CaM binding on CaM/IQ motif interaction. This may be the case if Ca^{2+} binding to CaM occurs in two steps. First, Ca^{2+}-free CaM (apoCaM) binds to the IQ motif and only then Ca^{2+} binds to CaM tethered to the IQ motif. This hypothesis is supported by numerous experimental data on binding of apoCaM to the IQ-like region [12–15].

Let us consider the following two-step scheme:

$$O + CaM \underset{k_{-1}}{\overset{k_1}{\Leftrightarrow}} O - CaM$$

$$O - CaM + Ca \underset{k_{-2}}{\overset{k_2}{\Leftrightarrow}} I - CaM - Ca \quad (7)$$

To show explicitly the dependence of the kinetic parameters of Ca^{2+} binding to CaM on CaM/IQ interaction, we suggest that the first step is faster than the second. In the simplest case of fast equilibrium between O and O-CaM (if $k_2 \cdot [Ca_{sch}]$, $k_{-2} < k_1$, k_{-1}), the two-step scheme (7) becomes

$$O^* + Ca \underset{k_{-2}}{\overset{k_2^*}{\Leftrightarrow}} I - CaM - Ca \tag{8}$$

where $O^* = O + O\text{-}CaM$; $O = O^*/(1 + [CaM]/K_1)$; $O\text{-}CaM = O \cdot [CaM]/K_1$; $K_1 = k_{-1}/k_1$;

$$k_2^* = k_2 \frac{[CaM]/K_1}{(1 + [CaM]/K_1)}.$$

In this case, the apparent constant (K_2^*) of Ca^{2+} dissociation from CaM depends on the dissociation constant K_1 and concentration of CaM as follows:

$$K_2^* = k_{-2}/k_2^* = \frac{k_{-2}(1 + [CaM]/K_1)}{k_2[CaM]/K_1}.$$

If the first allosteric site is actually CaM tethered to IQ motif, then the second site(s) regulated by Ca^{2+} from distant open channels (Ca_{sm}) may be the consensus EF hand motif or/and the peptide A region [13]. However, alternative possibilities that different Ca^{2+}-binding domains are the first or second allosteric sites for CDI cannot be excluded. The question is which of them (EF hand or CaM tethered to the peptide A or IQ-like motif) is the first site(s) and which is the second.

2.4. Changes in intracellular Ca^{2+} concentration near the membrane

Let us consider in more detail how the intracellular Ca^{2+} concentration near the membrane changes when calcium ions enter L-type Ca^{2+} channels. Note that when the channel is open, the concentration of Ca^{2+} strongly increases near the internal mouth of the open channel and moderately increases in a thin layer adjacent to the intracellular membrane surface near closed channels because of the lateral diffusion while the Ca^{2+} concentration in the cytosol changes little. Below the variable concentration of Ca^{2+} near open channels will be referred to as the microdomain (subchannel) concentration (Ca_{sch}), and the concentration of Ca^{2+} near closed channels will be referred to as the macrodomain (submebrane) concentration (Ca_{sm}).

2.4.1. Distribution of microdomain Ca^{2+}

Chad and Eckert [57] were the first to note that not only the calcium near the membrane but also perimembrane Ca^{2+} localized in domains adjacent to open channels is involved in CDI of Ca^{2+} channels. The Ca^{2+} concentration in these local domains is determined not by integral current but by the current through a single channel [57]. A theoretical analysis of the distribution of Ca^{2+} near the inner face of the membrane predicted that Ca^{2+} concentration in a local domain, a semisphere with a radius r with the center in the mouth of the open channel, can be hundreds of μM [58]. The Ca^{2+} concentration strongly increases to a stationary value when the channel opens and returns to bulk values when the channel is closed within as few as several microseconds at r of up to tens of nanometers. Later, these theoretical predictions received experimental support. It was shown using a low-sensitivity Ca^{2+} indicator that Ca^{2+} concentration in microdomains near open channels reaches values of 200–300 μM [59]. The distribution of Ca^{2+} near the open channel is most frequently described by the Neher equation [60]. Neher showed that in the presence of a mobile Ca^{2+}-binding buffer with a limited rate of calcium binding, the stationary distribution of Ca^{2+} concentration (c) with respect to the distance from the channel r is described by

$$c(r) = c_\infty + \frac{i\exp(-r/\lambda)}{4\pi FDr} \tag{9}$$

where c_∞ is the concentration of Ca^{2+} throughout the volume of the cytoplasm, i is the amplitude of the current through a single channel, F is the Faraday constant, D is the coefficient of Ca^{2+} diffusion in the cytoplasm, and λ is the effective length of Ca^{2+} buffering. $\lambda \approx [D^2/(k_{on} \cdot B)]^{1/2}$, where k_{on} is the constant of Ca^{2+} association with the buffer, B is the concentration of the mobile Ca^{2+} buffer. This equation was derived under the assumption that relative changes in the concentration of the buffer, free and bound to Ca^{2+}, are low compared with the changes in free Ca^{2+} and can be used under the conditions being of practical interest. More accurate solutions of the equations of diffusion in the case of a mobile Ca^{2+}-binding buffer were derived by Stern [61].

We shall describe the current through a single channel i by the Goldman–Hodgkin–Katz equation [62] unless otherwise indicated:

$$i = P_{Ca} F \left(\frac{F}{RT}\right) 2V \frac{Ca_{out}\exp\left(-\frac{2VF}{RT}\right) - Ca_{in}}{\exp\left(-\frac{2VF}{RT}\right) - 1}. \tag{10}$$

Here Ca_{out} and Ca_{in} ($Ca_{in}^{2+} \equiv c_\infty$) are invariable Ca^{2+} concentrations outside the cell and in the bulk of the cytoplasm, respectively, V is the membrane potential, P_{Ca} is the permeability coefficient of the single channel, F, R, and T have a common meaning. The potential outside the cell is taken as zero; therefore, the outward current will be considered as positive.

2.4.2. Distribution of macrodomain (submembrane) Ca^{2+}

For an infinite planar membrane, the stationary concentration of Ca^{2+} near the closed channel, which is determined by the lateral diffusion of Ca^{2+} from all adjacent open channels [63], can be calculated by integrating Eq. (9) with respect to r throughout the membrane surface. To do this, let

us assume that the closed channel is in the center of a membrane ring with a radius r and thickness dr. Then the stationary concentration of Ca^{2+} near that closed channel ($c_{sm}(r)$) will be determined by single currents i_r through N_r open channels in this ring by Eq. (4) in which $i_r = N_r \cdot i$ should be introduced instead of i. That is,

$$c_{sm}(r) = c_\infty + \frac{N_r i \exp(-r/\lambda)}{4\pi FDr} \quad (11)$$

Here $N_r = \sigma p_0 2\pi r dr$, where σ is the number of functionally active channels per 1 μm^2 of membrane surface, and p_0 is the channel open state probability.

The expression for the stationary concentration of Ca^{2+} near a closed channel (c_{sm}) at the expense of integral current through all open channels has the following form:

$$c_{sm} = c_\infty + \int_0^\infty \frac{N_r i \exp(-r/\lambda)}{4\pi FDr} = c_\infty + \frac{\sigma p_0 i \lambda}{2FD}. \quad (12)$$

It should be emphasized that this expression was derived for the case of uniform distribution of channels along the membrane surface. If the channels exist as clusters ("hot spots") largely separated from each other, as it is the case in L-type Ca^{2+} channels in cardiocytes [64], and the radius of a cluster R is less than λ, the equation for c_{sm} has the form

$$c_{sm} = c_\infty + \frac{\sigma p_0 i \lambda (1 - \exp(-R/\lambda))}{2FD} \quad (13)$$

or approximately

$$c_{sm} = c_\infty + \frac{\sigma p_0 i R}{2FD} \quad (14)$$

In this case, macrodomain concentration c_{sm} does not dependent on λ.

In further calculations, the following values of the fixed parameters were used: Ca_{out}=2000 μM; r=1 nm. The other parameters (D, λ, Ca_{in}, and σ) and the rate constants of channel switches were calculated by minimizing the deviations between the experimental and theoretical data. It was assumed in the calculations that Ca^{2+} concentration near open channels Ca_{sch} ($Ca_{sch} \equiv c(r)$) at a distance of 1 nm quickly (within a few microseconds) takes a stationary value equal to $c(r)$ at r=1 nm, which is determined by Eq. (9), where, instead of c_∞, the concentration of Ca^{2+} near the close channel, Ca_{sm}, is used. The variations of Ca_{sm} ($Ca_{sm} \equiv c_{sm}$) with time were described by the following expression:

$$\frac{d(Ca_{sm})}{dt} = \frac{\left(\frac{-\sigma \lambda i p_0}{2FD} + Ca_{in} - Ca_{sm}\right) D}{\lambda^2}. \quad (15)$$

Where D/λ^2 is the time constant for changes in Ca^{2+} concentration due to diffusion. This equation was derived for the following reason. The stationary value of Ca_{sm} satisfies Eq. (12), except that current i has the negative sign since this is an outward current. λ^2/D is the time constant of the diffusion process.

2.5. Computer simulations of the model

All computer simulations, including the solution of systems of differential and algebraic equations and fitting the experimental data to the model, were performed using the biochemical kinetics software packages Dbsolve [65]. The kinetic parameters for the model were calculated from the data on the time-course of either the whole-cell Ca^{2+} current [21] or the open state probability of single channels [66] using the non-linear least-squares method of minimization [67] implemented in the software package Dbsolve [65].

2.5.1. Initial conditions

In all simulations, to adjust the initial conditions, the system of differential equations was allowed to equilibrate at a holding potential. Model simulations of early and late openings [66] were performed using different initial conditions according to the experimental procedure of separation of all sweeps into early and late and by the normalization of open probability of all sweeps. The general initial condition in the system of equations describing the experiment [66] (Appendix B) corresponds to the steady state in this system at a holding potential of −50 mV. In this case, the total probability of all channel states is equal to unity. Early openings were calculated on assumption that the channel occurs initially only in active modes M_B and M_F; i.e., the probabilities of all states in inactive modes M_I, M_{Ca1}, and M_{Ca2} were taken to be equal to zero. The probabilities of all states in active modes M_B and M_F during late openings were assumed to be equal to zero. Thus, the total probability of being in all active and inactive modes was always equal to unity.

3. Results

Let us consider the key properties of the model based on the modal hypothesis of Ca^{2+}- and voltage-dependent transitions in the L-type Ca^{2+} channel. First of all, the model describes quantitatively whole-cell Ca^{2+} currents in molluscan neurons [21] in the control and in response to EGTA at different test potentials, i.e., at simultaneous changes in the membrane potential and intracellular Ca^{2+} concentration (Fig. 3).

The parameters of the model for which there is a good quantitative agreement between the experimental and simulation data are given in Table 1. All parameters, except λ and Ca_{in}, were the same in the control and in the presence of EGTA. In the control: λ=1 μm and Ca_{in}=50 nM. In the presence of EGTA, λ=0.012 μm and Ca_{in}^{2+}=1.4 nM.

To better understand the relationship between Ca^{2+} currents and the modes of channel behavior, Fig. 4 presents changes in the open state probability of the channel in

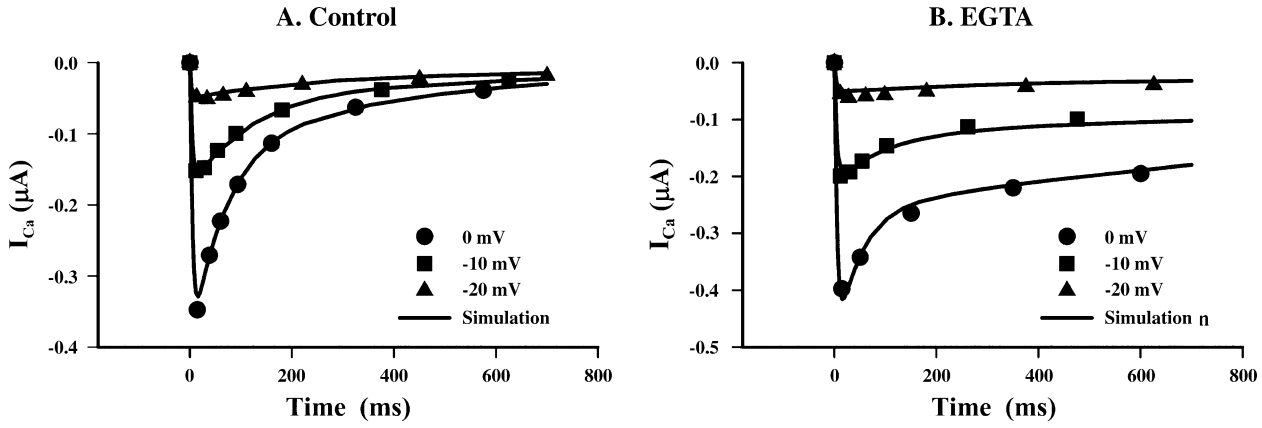

Fig. 3. Quantitative description of the experimental data on the kinetics of integral Ca currents in molluscan neurons [21]. Curves were obtained at different values of the test potential (0, −10, −20 mV) using the model of Ca-dependent inactivation. The holding potential is −40 mV. Circles, triangles, and squares represent experimental data, and solid lines denote the results of simulation. (A) Control; (B) in the presence of the Ca-binding buffer EGTA.

different active modes (M_B and M_F) and the redistribution between the modes at membrane depolarization. It is evident from Fig. 4A and B that the contributions of different modes to the total open state probability strongly depend on the concentration of the Ca^{2+} buffer. In the control, the total open state probability is almost entirely determined by the basal mode (Fig. 4A) since the contribution of the flickering mode is very small. After membrane depolarization, channels mainly switch to M_{Ca} (Fig. 4C). In the presence of EGTA, the contributions of both active modes (M_B and M_F) to the total open state probability of the channel become comparable (Fig. 4B) since, after membrane depolarization, the channels switch predominantly to the M_F mode (Fig. 4D). Here, it should be noted that, at low Ca^{2+} concentrations (EGTA), a slight slowing down of Ca^{2+} inactivation takes place. In this case, the inactivation time constant in the basal mode remains unchanged. The slowing down occurs due to a parallel increase in ^{F}O. Presumably, this is just the cause of the increase in the time constant of CDI, which is observed as Ca^{2+} concentration decreases in the nanomolar Ca^{2+} concentrations range [47,68]. At higher Ca^{2+} concentrations, the contribution of ^{F}O decreases, and the time constant of CDI does not change with increasing Ca^{2+} concentration, in full agreement with the experimental data.

To simulate the experimental data on mutations of different Ca^{2+}-binding domains in the CI region, we investigated Ca^{2+} currents at different values of association constant (k_{on}) of Ca^{2+} binding to the first and second allosteric sites. The results of simulation are presented in Fig. 5 and Table 2. One can see that the greatest changes in CDI result from changes in k_{on} of the first site (Fig. 5A). The 10-fold decrease in k_{on} (curve 2, Fig. 5A) results in a drastic (about sixfold) decrease in the time constant (τ_{Ca}) of CDI (Table 2). Further decrease in k_{on} (curves 3 and 4) results in a very slow inactivation of the channel. A saturation effect is observed at 100–1000-fold changes in k_{on} and the inactivation of the channel in this case can be described by the single slow component. The slowing down of CDI at mutations of the first allosteric site results from a very slow intermodal transition from the basal mode M_B to the inactive mode M_{Ca} at membrane depolarization (inset in Fig. 5A). By contrast, the simulation results show that 10-fold and greater changes in k_{on} of the second site lead to rather modest changes in CDI and drastic changes in VDI (Fig. 5B and Table 2). This interesting result is consistent with experimental data on the mutation of the consensus EF hand motif reported by Bernatchez et al. [54]. The strong slowing down of VDI results from the intermodal transition from M_B to the flickering mode M_F, which is believed to have very slow VDI (inset in Fig. 5B).

In addition, the model describes quantitatively two types of channel openings (Fig. 6): early openings (immediately after depolarization) with rapid inactivation and residual current and late openings (with a delay of a few tens of milliseconds) without inactivation. These patterns of channel opening were reported for single Ca^{2+} channels in cardiocytes [66] and have not yet been explained. The parameters of the model for which there is a good quantitative agreement between the experimental and simulation data are given in Table 1.

To better understand early and late openings in different modes, we analyzed experiments with double-pulse stimulation (Figs. 7–9) using the parameter values obtained by Rose et al. [66]. Initially, a prepulse from $V_h = -50$ mV to $V_m = -10$ mV of 1000-ms duration was applied (pulse 1), then the voltage was decreased to −100 mV for 20 ms before being returned to −10 mV (pulse 2).

Changes in the open state probability (the sum of early and late openings) in different modes during double-pulse stimulation are presented in Fig. 7. Fig. 7C shows that all openings in both active modes M_B and M_F during pulse 2 have lower amplitudes and a slower activation than during pulse 1. This is due to a strong fall of the amplitude in mode M_B (Fig. 7A) and an increased contribution of

Table 1
A detailed scheme of intra- and intermodal transitions in L-type Ca^{2+} channels

A detailed scheme of intramodal transitions

Equations for intramodal transitions	Description of experimental data [21]		Description of experimental data [66]	
	Constants of direct transition (ms^{-1})	Constants of reverse transition (ms^{-1})	Constants of direct transition (ms^{-1})	Constants of reverse transition (ms^{-1})
Mode B				
${}^{B}C_1 \Leftrightarrow {}^{B}C_2$	${}^{B}k_{C1,C2}\ {}^{B}\alpha_1=0.2$	${}^{B}k_{C2,C1}\ {}^{B}\alpha_1=0.2$	${}^{B}k_{C1,C2}\ {}^{B}\alpha_1=0.091$	${}^{B}k_{C2,C1}\ {}^{B}\alpha_1=0.091$
${}^{B}C_2 \Leftrightarrow {}^{B}O$	${}^{B}k_{C2,O}=2.5$	${}^{B}k_{O,C2}=0.63$	${}^{B}k_{C2,O}=0.22$	${}^{B}k_{O,C2}=1$
${}^{B}C_1 \Leftrightarrow {}^{B}I_1$	${}^{B}k_{C1,I1}=1.5\times10^{-3}$	${}^{B}k_{I1,C1}=1$	${}^{B}k_{C1,I1}=0.01$	${}^{B}k_{I1,C1}=1.25$
${}^{B}C_2 \Leftrightarrow {}^{B}I_2$	${}^{B}k_{C2,I2}=3\times10^{-3}$	${}^{B}k_{I2,C2}=1.6\times10^{-6}$	${}^{B}k_{C2,I2}=3.8\times10^{-3}$	${}^{B}k_{I2,C2}=5.5\times10^{-4}$
${}^{B}I_1 \Leftrightarrow {}^{B}I_2$	${}^{B}k_{I1,I2}\ {}^{B}\alpha_2=0.04$	${}^{B}k_{I2,I1}\ {}^{B}\alpha_2=0.04$	${}^{B}k_{I1,I2}\ {}^{B}\alpha_2=0.065$	${}^{B}k_{I2,I1}\ {}^{B}\alpha_2=0.065$
Mode I				
${}^{I}C_1 \Leftrightarrow {}^{I}C_2$	${}^{I}k_{C1,C2}\ {}^{I}\alpha_1=0.2$	${}^{I}k_{C2,C1}\ {}^{I}\alpha_1=0.2$	${}^{I}k_{C1,C2}\ {}^{I}\alpha_1=0.91$	${}^{I}k_{C2,C1}\ {}^{I}\alpha_1=0.091$
${}^{I}C_2 \Leftrightarrow {}^{I}I_3$	${}^{I}k_{C2,I3}=2.5$	${}^{I}k_{I3,C2}=0.63$	${}^{I}k_{C2,\ I3}=0.22$	${}^{I}k_{I3,C2}=1$
${}^{I}C_1 \Leftrightarrow {}^{I}I_1$	${}^{I}k_{C1,I1}=1.5\times10^{-3}$	${}^{I}k_{I1,C1}=1$	${}^{I}k_{C1,I1}=0.01$	${}^{I}k_{I1,C1}=1.25$
${}^{I}C_2 \Leftrightarrow {}^{I}I_2$	${}^{I}k_{C2,I2}=3\times10^{-3}$	${}^{I}k_{I2,C2}=1.6\times10^{-6}$	${}^{I}k_{C2,I2}=3.8\times10^{-3}$	${}^{I}k_{I2,C2}=5.5\times10^{-4}$
${}^{I}I_1 \Leftrightarrow {}^{I}I_2$	${}^{I}k_{I1,I2}\ {}^{I}\alpha_2=0.04$	${}^{I}k_{I2,I1}\ {}^{I}\alpha_2=0.04$	${}^{I}k_{I1,I2}\ {}^{I}\alpha_2=0.065$	${}^{I}k_{I2,I1}\ {}^{I}\alpha_2=0.065$
Mode F				
${}^{F}C_1 \Leftrightarrow {}^{F}C_2$	${}^{F}k_{C1,C2}\ {}^{F}\alpha_1=0.2$	${}^{F}k_{C2,C1}\ {}^{F}\alpha_1=0.2$	${}^{F}k_{C1,C2}\ {}^{F}\alpha_1=0.91$	${}^{F}k_{C2,C1}\ {}^{F}\alpha_1=0.091$
${}^{F}C_2 \Leftrightarrow {}^{F}O$	${}^{F}k_{C2,O}=0.63$	${}^{F}k_{O,C2}=0.75$	${}^{F}k_{C2,O}=5$	${}^{F}k_{O,C2}=1.5$
Mode Ca				
${}^{Ca1}C_1 \Leftrightarrow {}^{Ca1}C_2$	${}^{Ca1}k_{C1,C2}\ {}^{Ca1}\alpha_1=0.2$	${}^{Ca1}k_{C2,C1}\ {}^{Ca1}\alpha_1=0.2$	${}^{Ca1}k_{C1,C2}\ {}^{Ca1}\alpha_1=0.91$	${}^{Ca1}k_{C2,C1}\ {}^{Ca1}\alpha_1=0.091$
${}^{Ca1}C_2 \Leftrightarrow {}^{Ca1}I_3$	${}^{Ca1}k_{C2,I3}=2.5$	${}^{Ca1}k_{I3,C2}=0.63$	${}^{I}k_{C2,\ I3}=0.22$	${}^{Ca1}k_{I3,C2}=1$
${}^{Ca1}C_1 \Leftrightarrow {}^{Ca1}I_1$	${}^{Ca1}k_{C1,I1}=0.2$	${}^{Ca1}k_{I1,C1}=0.1$	${}^{I}k_{C1,I1}=0.01$	${}^{Ca1}k_{I1,C1}=1.25$
${}^{Ca1}C_2 \Leftrightarrow {}^{Ca1}I_2$	${}^{Ca1}k_{C2,I2}=8\times10^{-3}$	${}^{Ca1}k_{I2,C2}=3\times10^{-8}$	${}^{Ca1}k_{C2,I2}=3.8\times10^{-3}$	${}^{Ca1}k_{I2,C2}=5.5\times10^{-4}$
${}^{Ca1}I_1 \Leftrightarrow {}^{Ca1}I_2$	${}^{Ca1}k_{I1,I2}\ {}^{Ca1}\alpha_2=0.04$	${}^{Ca1}k_{I2,I1}\ {}^{Ca1}\alpha_2=0.04$	${}^{Ca1}k_{I1,I2}\ {}^{Ca1}\alpha_2=0.065$	${}^{Ca1}k_{I2,I1}\ {}^{Ca1}\alpha_2=0.065$
${}^{Ca2}C_1 \Leftrightarrow {}^{Ca2}C_2$	${}^{Ca2}k_{C1,C2}\ {}^{Ca2}\alpha_1=0.2$	${}^{Ca2}k_{C2,C1}\ {}^{Ca2}\alpha_1=0.2$	${}^{Ca2}k_{C1,C2}\ {}^{Ca2}\alpha_1=0.91$	${}^{Ca2}k_{C2,C1}\ {}^{Ca2}\alpha_1=0.091$
${}^{Ca2}C_2 \Leftrightarrow {}^{Ca2}I_3$	${}^{Ca2}k_{C2,I3}=2.5$	${}^{Ca2}k_{I3,C2}=0.63$	${}^{Ca2}k_{C2,I3}=0.22$	${}^{Ca2}k_{I3,C2}=1$
${}^{Ca2}C_1 \Leftrightarrow {}^{Ca2}I_1$	${}^{Ca2}k_{C1,I1}=0.2$	${}^{Ca2}k_{I1,C1}=0.1$	${}^{Ca2}k_{C1,I1}=0.01$	${}^{Ca2}k_{I1,C1}=0.95$
${}^{Ca2}C_2 \Leftrightarrow {}^{Ca2}I_2$	${}^{Ca2}k_{C2,I2}=8\times10^{-3}$	${}^{Ca2}k_{I2,C2}=3\times10^{-8}$	${}^{Ca2}k_{C2,I2}=3.8\times10^{-3}$	${}^{Ca2}k_{I2,C2}=3\times10^{-4}$
${}^{Ca2}I_1 \Leftrightarrow {}^{Ca2}I_2$	${}^{Ca2}k_{I1,I2}\ {}^{Ca2}\alpha_2=0.4$	${}^{Ca2}k_{I2,I1}\ {}^{Ca2}\alpha_2=0.4$	${}^{Ca2}k_{I1,I2}\ {}^{Ca2}\alpha_2=0.065$	${}^{Ca2}k_{I2,I1}\ {}^{Ca2}\alpha_2=0.065$

A detailed scheme of intermodal Ca^{2+}-dependent transitions

Equations for intermodal transitions	Description of experimental data [21]		Description of experimental data [66]	
	Constants of direct transition ($\mu M^{-1}\ ms^{-1}$)	Constants of reverse transition (ms^{-1})	Constants of direct transition ($\mu M^{-1}\ ms^{-1}$)	Constants of reverse transition (ms^{-1})
${}^{B}C_1+Ca_{sm} \Leftrightarrow {}^{I}C_1$	${}^{C1}l_{B,I}=1.5\times10^{-4}$	${}^{C1}l_{I,B}=0.45$	${}^{C1}l_{B,I}=2.2\times10^{-4}$	${}^{C1}l_{I,B}=0.22$
${}^{B}C_2+Ca_{sm} \Leftrightarrow {}^{I}C_2$	${}^{C2}l_{B,I}=1.5\times10^{-4}$	${}^{C2}l_{I,B}=0.45$	${}^{C2}l_{B,I}=2.2\times10^{-4}$	${}^{C2}l_{I,B}=0.22$
${}^{B}O+Ca_{sch} \Leftrightarrow {}^{I}I_3$	${}^{O}l_{B,I}=1.5\times10^{-4}$	${}^{O}l_{I,B}=0.45$	${}^{O}l_{B,I}=2.2\times10^{-4}$	${}^{O}l_{I,B}=0.22$
${}^{I}C_1+Ca_{sm} \Leftrightarrow {}^{Ca1}C_1$	${}^{C1}l_{I,Ca1}=10$	${}^{C1}l_{Ca1,I}=10$	${}^{C1}l_{I,Ca1}=10$	${}^{C1}l_{Ca1,I}=1$
${}^{I}C_2+Ca_{sm} \Leftrightarrow {}^{Ca1}C_2$	${}^{C2}l_{I,Ca1}=10$	${}^{C2}l_{Ca1,I}=10$	${}^{C2}l_{I,Ca1}=10$	${}^{C2}l_{Ca1,I}=1$
${}^{I}I_3+Ca_{sm} \Leftrightarrow {}^{Ca1}I_3$	${}^{I3}l_{I,Ca1}=10$	${}^{I3}l_{Ca1,I}=10$	${}^{I3}l_{I,Ca1}=10$	${}^{I3}l_{Ca1,I}=1$

A detailed scheme of Ca-independent intermodal transitions

Equations for intermodal transitions	Description of experimental data [21]		Description of experimental data [66]	
	Constants of direct transition (ms^{-1})	Constants of reverse transition (ms^{-1})	Constants of direct transition (ms^{-1})	Constants of reverse transition (ms^{-1})
${}^{I}C_1 \Leftrightarrow {}^{F}C_1$	${}^{C1}l_{I,F}=0.5$	${}^{C1}l_{F,I}=3.3\times10^{-3}$	${}^{C1}l_{I,F}=0.8$	${}^{C1}l_{F,I}=0.053$
${}^{I}C_2 \Leftrightarrow {}^{F}C_2$	${}^{C2}l_{I,F}=0.5$	${}^{C2}l_{F,I}=3.3\times10^{-3}$	${}^{C2}l_{I,F}=0.8$	${}^{C2}l_{F,I}=0.053$
${}^{I}I_3 \Leftrightarrow {}^{F}O$	${}^{I3}l_{I,F}=0.5$	${}^{I3}l_{F,I}=3.3\times10^{-3}$	${}^{I3}l_{I,F}=0.8$	${}^{I3}l_{F,I}=0.053$
${}^{Ca1}C_1 \Leftrightarrow {}^{Ca2}C_1$	${}^{C1}l_{Ca1,Ca2}=4$	${}^{C1}l_{Ca2,Ca1}=0.023$	${}^{C1}l_{Ca1,Ca2}=44$	${}^{C1}l_{Ca2,Ca}=0.11$
${}^{Ca1}C_2 \Leftrightarrow {}^{Ca2}C_2$	${}^{C2}l_{Ca1,Ca2}=4$	${}^{C2}l_{Ca2,Ca1}=0.023$	${}^{C2}l_{Ca1,Ca2}=44$	${}^{C2}l_{Ca2,Ca1}=0.11$
${}^{Ca1}I_3 \Leftrightarrow {}^{Ca2}I_3$	${}^{I3}l_{Ca1,Ca2}=4$	${}^{I3}l_{Ca2,Ca1}=0.023$	${}^{I3}l_{Ca1,Ca2}=44$	${}^{I3}l_{Ca2,Ca1}=0.11$

The rest parameters are: For data Chad et al. [15]: $V_1=4.6$ mV; $V_2=-70$ mV; $K=5.33$ mV; $P_{Ca}*F=10^{-5}$ pA/μM; $D_{Ca}=0.6$ μm^2 ms^{-1}; $\sigma=5.8$ μm^{-2}; $S=1.2\times10^6$ μm^2.
For data Rose et al. (1992): $V_1=-22.8$ mV; $V_2=-70.2$ mV; $K=7$ mV; $g_{Ca}=6.9$ pS; $D_{Ca}=0.15$ μm^2 ms^{-1}.

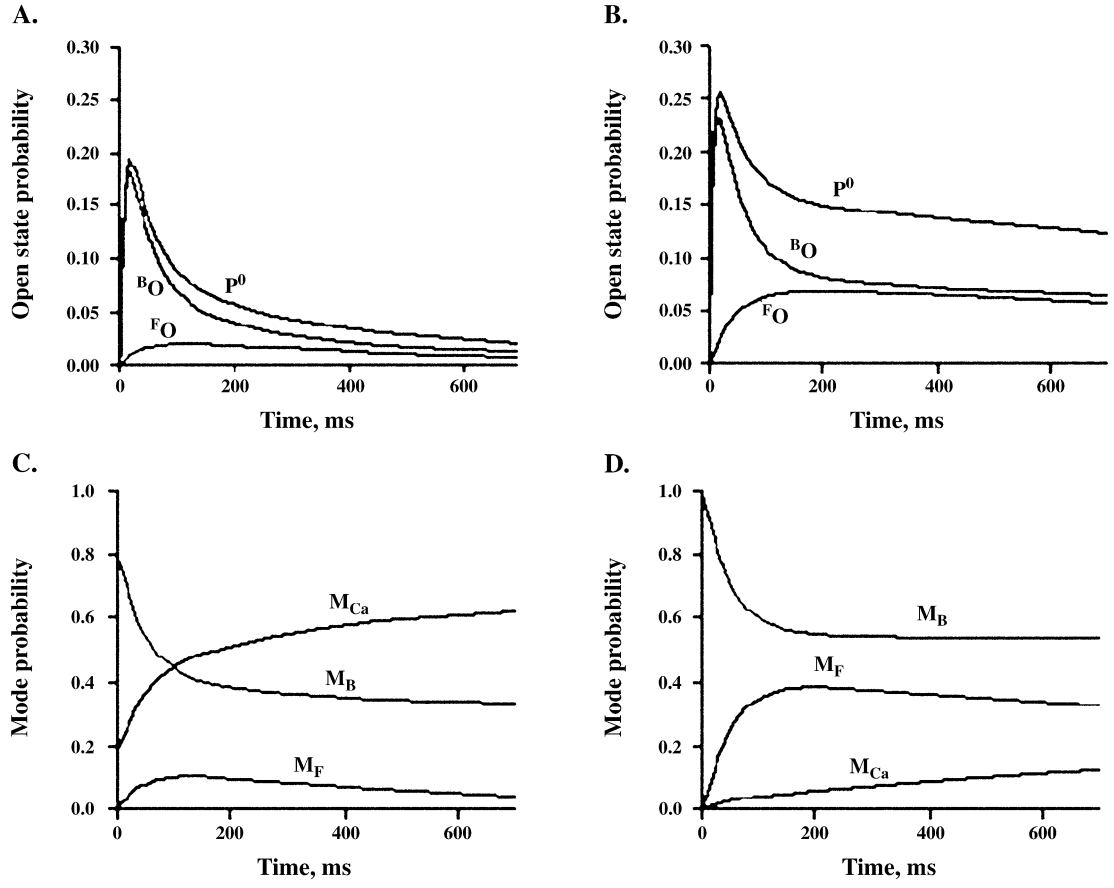

Fig. 4. Changes in the channel open state probability with time and the kinetics of different mode probability in the control (A, C) and in the presence of EGTA (B, D). Total open state probability $p_o = {}^{B}O + {}^{F}O$ is the sum of two open state probabilities, ${}^{B}O$ and ${}^{F}O$, while M_B, M_F and M_{Ca} are the sums of all the state probabilities in respective modes. The conditions are as in Fig. 3.

openings in mode M_F (Fig. 7B). More detailed changes in channel opening during the prepulse are seen in Figs. 8 and 9, which show early and late openings in different modes. It is interesting that the late openings can be accounted for by intermodal transitions of the channel. A delay in the late openings results from the slow transition

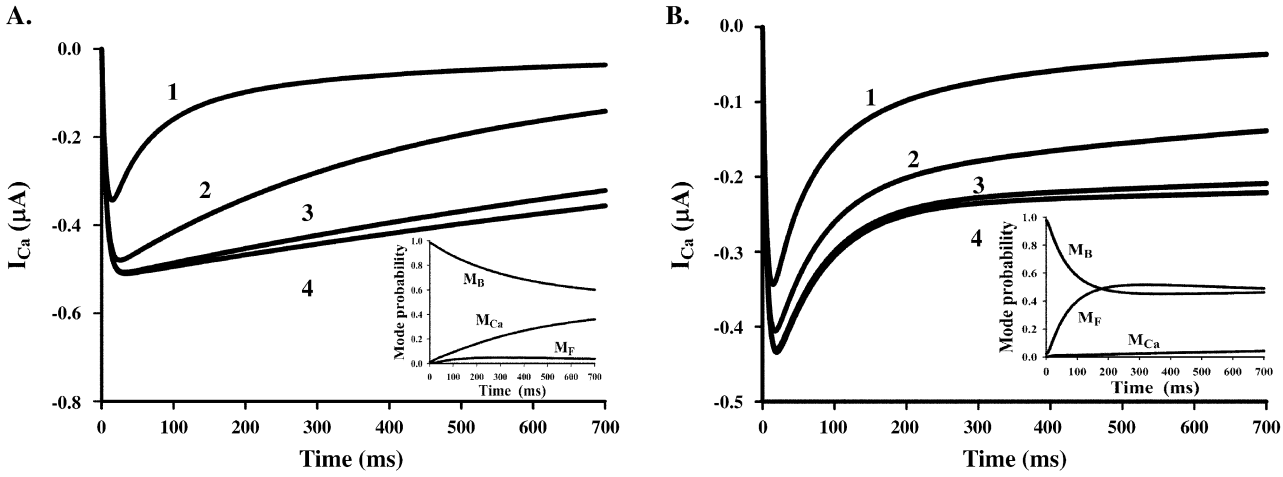

Fig. 5. Ca^{2+} currents at simulation of mutations of the first and second allosteic sites. Curves were obtained at following values of association constant of Ca^{2+} binding to the first (A) and second (B) sites: (A) ${}^{O}l_{B,I} = {}^{C1}l_{B,I} = {}^{C2}l_{B,I} = 1.5 \times 10^{-4}$, 1.5×10^{-5}, 1.5×10^{-6}, and 1.5×10^{-7} μM^{-1} ms^{-1} for curves 1, 2, 3, and 4, respectively. (B) ${}^{I3}l_{I,Ca1} = {}^{C1}l_{I,Ca1} = {}^{C2}l_{I,Ca1} = 10$, 1, 0.1, and 0.01 μM^{-1} ms^{-1} for curves 1, 2, 3, and 4, respectively. Time course of modes probability is shown as inserts. Inset in (A) corresponds to curve 2, and in (B) curve 4. Curve 1 in (A) and (B) corresponds to control parameter values.

Table 2
Kinetics of I_{Ca} inactivation at simulation of mutation of allosteric sites

Association constant (μM^{-1} ms^{-1})	A_{Ca} (μA)	τ_{Ca} (ms)	A_V (μA)	τ_V (ms)	I_0 (μA)
Simulation of mutation of the first allosteric site					
1.5×10^{-4}	0.29	56	0.12	403	0.014
1.5×10^{-5}	0.20	297	0.30	689	0.014
1.5×10^{-6}	–	–	0.48	1313	0.04
1.5×10^{-7}	–	–	0.48	1668	0.04
Simulation of mutation of the second allosteric site					
10	0.29	56	0.12	403	0.014
1	0.26	63	0.12	565	0.011
0.1	0.27	70	0.06	840	0.18
0.01	0.27	72	0.06	1737	0.19

Inactivation kinetics of I_{Ca} were fitted with the double-exponential function: $-I_{Ca}(t)=A_{Ca}\times\exp(-t/\tau_{Ca})+A_V\times\exp(-t/\tau_V)+I_0$, except the simulation of mutations of the first site at association constants ${}^{O}l_{B,I}={}^{C1}l_{B,I}={}^{C2}l_{B,I}=1.5\times10^{-6}$, 1.5×10^{-7} μM^{-1} ms^{-1}. These simulation mutations corresponding curves 3 and 4 in Fig. 5A were well described by a single exponential.

from the inactive modes M_{Ca} and M_I to the active modes M_B and M_F. The main conclusion that can be derived from these figures is the following. In the control (pulse 1), late openings are related to intermodal transitions from the inactive modes M_I and M_{Ca} to the active mode M_F since the amplitude of late openings in mode M_B is neglected (Fig. 9A). After the prepulse, the number of early openings during pulse 2 drastically diminishes due to a decrease in the probability of openings in mode M_B (Fig. 8A). The amplitude of late openings during pulse 2 strongly increases due to an increase in the probability of openings in mode M_F (Fig. 9B).

It is interesting that the calculated rate constant for the entry of the channel into the open state in cardiocytes (see Table 1) in mode M_F is much higher than the analogous rate constant in mode M_B (${}^{F}k_{C2,O}=5$, ${}^{B}k_{C2,O}=0.22$ ms^{-1}). The rate constant $k_{O,C2}$ changes only slightly in these modes. This means that the channel open probability in mode M_F is much higher than in mode M_B at equal conditions. Thus, mode M_F may be considered as a facilitation mode [1].

4. Discussion

Initially, the hypothesis of the presence of two different allosteric sites and a strict order of binding of Ca^{2+} to these sites was based on experimental data on the kinetics of inactivation of L-type Ca^{2+} currents. Recent investigations in molecular biology supported the hypothesis that there are at least two different Ca^{2+}-binding sites that determine the CDI in the C-terminal tail (residues 1520–1732) of the pore-forming α_1-subunit of L-type Ca^{2+} channels [5–15]. Based on the hypothesis of Peterson et al. [11], we proposed that the first site, which binds local Ca^{2+} immediately after the channel opening, is CaM tethered to the IQ-like motif. In this case, the second site(s) regulated by Ca^{2+} from distant open channels (Ca_{sm}) may be the consensus EF hand motif or/and CaM tethered to the CI region labeled peptide LM1 [12] or peptide A [13].

In principle, we do not insist on this distribution of roles among allosteric sites. For example, EF hand might be the first allosteric site. In this case, the binding of Ca^{2+} to CaM tethered to the IQ-like or peptide A motif may fulfil an auxiliary function, stabilizing the inactivated state and completing the CDI process. One reason for the modest influence of mutations in the Ca^{2+}-coordinating center of the EF hand on CDI might not be the classical mechanism of binding Ca^{2+} to the consensus EF hand motif [52]. That is why it is difficult to evaluate a decrease in the Ca^{2+} dissociation constant upon the mutations.

Besides, an alternative hypothesis about the first allosteric site regulated by local Ca^{2+} could be that a very attractive target for local Ca_{sch} is also CaM tethered to 1591TLF1593 and 1595LVR1597 sequences of the peptide A of the CI region [15]. It is very important that these sequences can bind Ca^{2+}-free CaM (apoCaM) and drastically change CDI. Besides, these domains are located near the consensus EF hand motif and this proximity can provide the development of fast CDI if the EF hand actually only supports CDI [11].

The results of our mutation simulation show that mutations in the first site, regulated by local Ca_{sch}, lead to

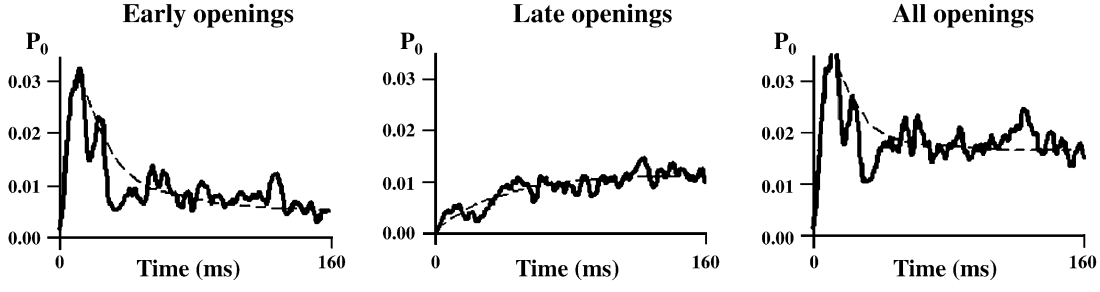

Fig. 6. Quantitative description of the experimental data on the kinetics of elementary currents on single Ca^{2+} channels of cardiocytes [66]. Solid lines denote the theoretical data, and thin lines denote experimental data. The holding potential is −50 mV and test potential is −10 mV. Differential equations are given in Appendix B. Most of the parameter values are given in Table 1. The remaining parameters are $V_1=-22.8$ mV; $V_2=-70.2$ mV; $\kappa=7$ mV; $D_{Ca}=0.15$ μm^2 ms^{-1}; $g_{Ca}=6.9$ pS; $Ca_{in}=40$ nM; $\lambda=1$ μm; $\sigma=1.7$ μm^{-2}.

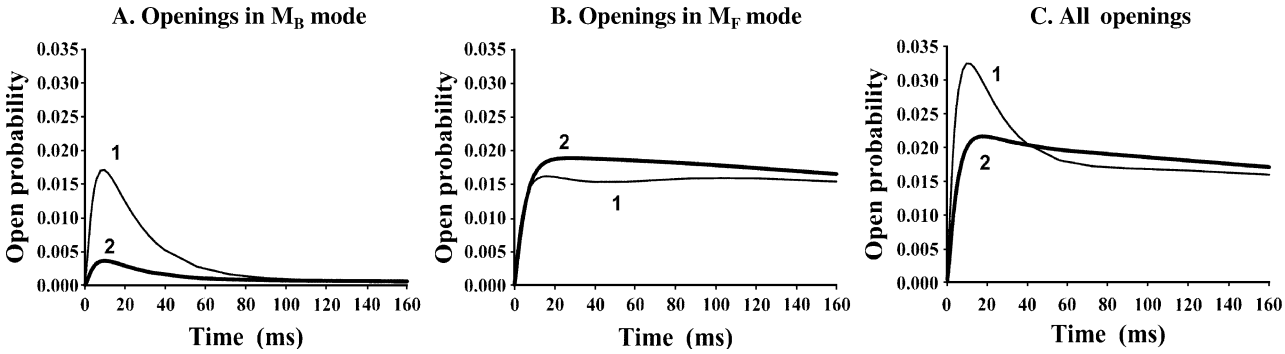

Fig. 7. Simulation results on open probability of all openings in different modes during double-impulse stimulation. Curves 1 and 2 correspond to prepulse from $V_h = -50$ mV to $V_m = -10$ mV of duration of 1000 ms and test pulse, respectively. The conditions are as in Fig. 6.

drastic changes in the time constant of CDI (Fig. 5A). By contrast, mutations in the second site result in modest changes in CDI, whereas VDI changes very strongly (Fig. 5B).

We believe that these simulation results can help solve the question as to which of Ca^{2+}-binding sites is the first site(s) and which is the second. It is very important that binding of local Ca_{sch} to the first site initiates CDI and determines its time constant. Therefore, experimental mutations in the first site should primarily lead to changes in the CDI time constant. The binding of Ca^{2+} to the second site occurs only after the inactivation of the channel. In this case, the binding of Ca^{2+} to the second site stabilizes CDI. Thus, experimental mutations of the second site should result in modest CDI changes and drastic VDI changes. Therefore, it is very useful to compare our simulation results with experimental data on mutations of different CI domains. Our results on the simulation of mutations of the second allosteric site (Fig. 5B) are consistent with experimental mutations of the EF hand motif [11,54] and the 1595LVR1597 domain of peptide A region [15]. These simulation and experimental data show, first, mutations have a modest influence on CDI and, second, they influence mainly the amplitude of CDI but not the time constant. Therefore, these data support the hypothesis that the EF hand and the 1595LVR1597 domain are the second allosteric site for CDI. Besides, our results on simulation of mutations of the first allosteric site (Fig. 5A) are compatible with the experimental data on mutations of the IQ motif [9,10,16,56] and support the hypothesis that the IQ is the first allosteric site. However, the experimental data on mutations of different amino acid residues of the IQ region show a more complicated influence on the inactivation of the L-type Ca channel. These mutations can also give rise to changes in Ca^{2+}-dependent facilitation [16,56] and acceleration of Ba^{2+} inactivation [8,14,15,56]. Therefore, our description of the initial step of CDI as a simple binding of local Ca_{sch} to the first allosteric site (IQ motif) to induce CDI is oversimplified. Presumably, there are other key kinetic steps including facilitation and fast Ca^{2+}-independent inactivation accompanying CDI, which are not considered in our model.

Some concern may be because of our attempt to combine the two models, "shell" and "domain," in a single kinetic mechanism. Actually, the "shell" model was proposed mostly for Ca^{2+} channels in invertebrates, while the "domain" model was used to describe the main features of inactivation in Ca^{2+} channels of higher animals. For instance, in Aplysia neurons, inactivation of whole cell calcium currents is significantly accelerated by intracellular calcium in the 1 μM range, while in vertebrates, this effect is much less pronounced, or it requires much higher concentrations [69]. However, these differences can be explained in the frame of our combine model. Our calculations show (Eq. (14)) that the macrodomain Ca^{2+} concentration does not dependent on even fast chelators of Ca^{2+} if the channels exist as clusters ("hot spots"), as it is the case in L-type Ca^{2+} channels in cardiocytes [64]. That is why CDI of L-type Ca^{2+} channels in vertebrates can show insignificant

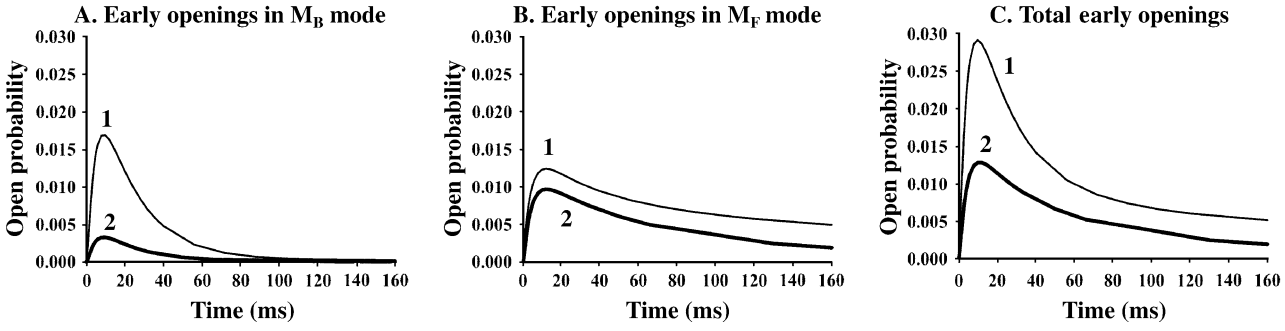

Fig. 8. Simulation results on open probability of early openings in different modes at double-impulse stimulation. The conditions are as in Fig. 7.

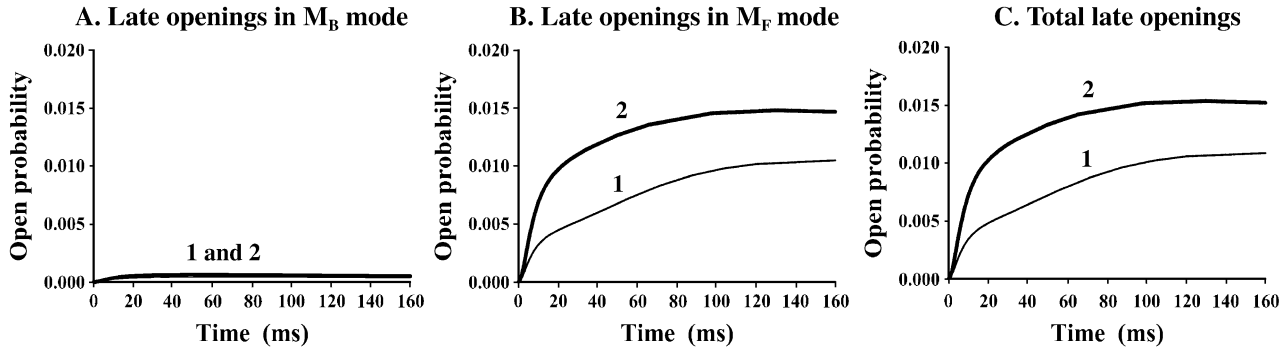

Fig. 9. Simulation results on open probability of late openings in different modes at double-impulse stimulation. The conditions are as in Fig. 7.

dependence on Ca^{2+}-binding buffer concentration and have the purely "domain" model features.

Anyway, the suggested kinetic model explains the following important kinetic features of rapid voltage- and Ca^{2+}-dependent regulation of Ca^{2+} channels, which were thus far unclear or have been misinterpreted.

(1) It was shown experimentally that the acceleration of inactivation of Ca^{2+} channels induced by increasing intracellular Ca^{2+} concentration is not due to a decrease in the time constants of Ca^{2+}- and potential-dependent inactivation (τ_{Ca} and τ_V), but mainly to a greater contribution of fast inactivation compared to slow inactivation, i.e., an increase in the $A_{Ca}/(A_{Ca}+A_V)$ ratio, where A_{Ca} and A_V are the amplitudes of Ca^{2+}- and potential-dependent inactivations [47,68]. As Ca^{2+} concentration was increased from 1 nM to about 50 nM, τ_{Ca} decreased only slightly and then remained unchanged on further increase in Ca^{2+} concentration. This is in complete agreement with our model in which τ_{Ca} depends only on Ca_{sch}, and A_{Ca} depends on Ca^{2+}_{sm}. A decrease in the time constant of CDI in the nanomolar Ca^{2+} concentrations range can be explained by the fact that CDI occurs parallel with the increase in open probability (^FO) in the flickering mode M_F (Fig. 4). At higher Ca^{2+} concentrations, the contribution of ^FO decreases, and T_{Ca} does not change with increasing Ca^{2+} concentration, in full agreement with the experimental data.

(2) The experimental data show that the amplitude of CDI, A_{Ca}, increases with increasing density of channels in the membrane [37,70]. The model explains this finding as follows. A_{Ca} depends on the concentration of Ca^{2+} arising from distant open channels (Ca_{sm},) and increases with increasing channel density.

(3) In the case of the two-pulse stimulation protocol, the exit from channel inactivation during membrane hyperpolarization after the prepulse slows down strongly as intracellular Ca^{2+} concentration increases [3]. The model explains this finding as follows. As intracellular Ca^{2+} concentration increases, the inactivation proceeds by the Ca^{2+}-dependent mechanism, i.e., through the transition from M_B to M_I and then to M_{Ca}. The recovery from inactivation is associated with the reverse transition from M_{Ca} to M_B, which proceeds much more slowly (hundreds of milliseconds) at high Ca^{2+} concentration.

(4) After the second impulse, which is preceded by a prepulse, the Ca^{2+} current has a low amplitude (channels are partly inactivated) and is inactivated mainly by the mechanism of slow potential-dependent regulation. It follows from the analysis of our model that it is not quite correct to relate slow inactivation only to the slight increase in intracellular Ca^{2+} concentration at a small amplitude of Ca^{2+} current. The calculations show that the fast inactivation component can also be observed at very low intracellular Ca^{2+} concentrations. For this to occur, the rate constants of transition between M_I and M_F should favour the transition to M_F. Channels with such a high equilibrium constant exhibiting a higher level of residual current. In this case, the transition from M_B to M_F during membrane depolarization proceeds via the inactive intermediate mode M_I, and consequently, the fast inactivation component will be present, though with a low amplitude, even at a very low Ca^{2+} concentration. Experiments with barium as a carrier of current through L-type Ca^{2+} channels revealed a fast inactivation component related to phosphorylation of the channels [41]. Therefore, the model proposes a different explanation for the data using a two-pulse stimulation protocol. After a prepulse, the channels transit from M_B to M_I and M_{Ca}. After a short (about 10 ms) hyperpolarizing pulse before the second depolarizing pulse, the equilibrium between M_{Ca}, M_I, and M_B remains practically unchanged because the reverse transition requires a few tens of milliseconds. It is for this reason that no changes in the redistribution of channels between modes M_B, M_I, and M_{Ca} (these

modes are in equilibrium) occur after repeated depolarization. Consequently, no CDI takes place, and the channels are inactivated only by the slow potential-dependent mechanism within one mode, M_B.

(5) Single channels exhibit two patterns of opening: early openings with rapid inactivation and residual current, which occur immediately after depolarization, and later openings without inactivation, which occur with a delay of several tens of milliseconds after the onset of depolarization (Fig. 6). Some authors relate these patterns of channel behavior to different degrees of channel phosphorylation. Our model quantitatively describes the probability of early and late openings of open channels. Early openings are determined by the total channel opening probability in active modes M_B and M_F, where the channel originally exhibits these modes of behavior. Late openings are determined by the initial total probability of channel being in inactive modes M_{Ca} and M_I. The first latency is just associated with the transition from inactive modes to M_F. The results of the calculations suggest that the channel states characterized by early and late openings can be considered as different short-lived modes and the transitions between these modes Ca^{2+}-dependent.

(6) Experiments with two-pulse stimulation of single Ca^{2+} channels also showed that during depolarization, channel opening that follows a prepulse occurs after a substantial delay (up to a few tens of milliseconds) [27]. It is on the basis of these experiments that the hypothesis of Ca^{2+}-dependent inactivation with two modes of channel behavior, M_B (basal mode) and M_{Ca} (Ca^{2+}-dependent mode) was proposed. The model with two modes does not explain the results of the experiments in which the first opening of the channel (which proceeds with a great delay) is practically always followed by frequent openings and closings in the form of short bursts of pulses. In our model, these data are accounted for by a slow transition from the inactive mode M_{Ca} to the flickering mode M_F.

4.1. Predictions

Let us now dwell on the predictions of the kinetic model of fast regulation. The model predicts that delayed openings of a single channel during depolarization without prepulse are mainly associated with the transition from mode M_{Ca} to M_F. By varying the initial values of Ca^{2+} concentration in M_{Ca}, it is possible to change the probability of late openings. Delayed openings will not be observed at least in two cases. First, if the holding potential is about −100 mV, the channel will be originally in mode M_B, and only early openings with fast inactivation and residual current will be generated under depolarization. Second, at very low Ca^{2+} concentrations (a few nanomoles), the probability for the channel being in mode M_{Ca} is also very low, and delayed openings will not occur.

The occurrence of intermodal transitions from M_{Ca} to M_F can also be established also on integral currents by regulating the portion of channels being in mode M_{Ca}. The model predicts that only channels that are originally in mode M_B can be inactivated by the Ca^{2+}-dependent mechanism. Therefore, after applying a depolarizing prepulse from the holding potential of −100 mV where all channels are in mode M_B and are not inactivated at high intracellular Ca^{2+} concentration, almost all channels will switch from mode M_B to mode M_{Ca}. The second pulse applied after a short (10 ms) hyperpolarization restores channels in M_{Ca} from potential-dependent inactivation, which should only lead to a slowly increasing current related to slow transition of the channel from mode M_{Ca} to M_F.

Acknowledgments

We are grateful to Jan B. Hoek, Michael E. O'Leary, Michele Solem, and Svetlana V. Sidorova for critically reading the manuscript. This work was supported by grants from the Russian Foundation for Basic Research (projects 00-04-49199 to NIM and 04-04-48658 to YMK).

Appendix A. Intra- and intermodal transitions in L-type Ca^{2+} channels

Table A1
A detailed scheme and equations for intra- and intermodal transitions in L-type Ca^{2+} channels

Number	Elementary steps	Equations for transition rates
Intramodal transitions		
	Mode B	
1	${}^{B}C_1 \Leftrightarrow {}^{B}C_2$	$v_1 = {}^{B}k_{C1,C2} \cdot {}^{B}C_1 - {}^{B}k_{C2,C1} \cdot {}^{B}C_2$
2	${}^{B}C_2 \Leftrightarrow {}^{B}O$	$v_2 = {}^{B}k_{C2,O} \cdot {}^{B}C_2 - {}^{B}k_{O,C2} \cdot {}^{B}O$
3	${}^{B}C_1 \Leftrightarrow {}^{B}I_1$	$v_3 = {}^{B}k_{C1,I1} \cdot {}^{B}C_1 - {}^{B}k_{I1,C1} \cdot {}^{B}I_1$
4	${}^{B}C_2 \Leftrightarrow {}^{B}I_2$	$v_4 = {}^{B}k_{C2,I2} \cdot {}^{B}C_2 - {}^{B}k_{I2,C2} \cdot {}^{B}I_2$
5	${}^{B}I_1 \Leftrightarrow {}^{B}I_2$	$v_5 = {}^{B}k_{I1,I2} \cdot {}^{B}I_1 - {}^{B}k_{I2,I1} \cdot {}^{B}I_2$
	Mode I	
6	${}^{I}C_1 \Leftrightarrow {}^{I}C_2$	$v_6 = {}^{I}k_{C1,C2} \cdot {}^{I}C_1 - {}^{I}k_{C2,C1} \cdot {}^{I}C_2$
7	${}^{I}C_2 \Leftrightarrow {}^{I}I_3$	$v_7 = {}^{I}k_{C2,O} \cdot {}^{I}C_2 - {}^{I}k_{O,C2} \cdot {}^{I}I_3$
8	${}^{I}C_1 \Leftrightarrow {}^{I}I_1$	$v_8 = {}^{I}k_{C1,I1} \cdot {}^{I}C_1 - {}^{I}k_{I1,C1} \cdot {}^{I}I_1$
9	${}^{I}C_2 \Leftrightarrow {}^{I}I_2$	$v_9 = {}^{I}k_{C2,I2} \cdot {}^{I}C_2 - {}^{I}k_{I2,C2} \cdot {}^{I}I_2$
10	${}^{I}I_1 \Leftrightarrow {}^{I}I_2$	$v_{10} = {}^{I}k_{I1,I2} \cdot {}^{I}I_1 - {}^{I}k_{I2,I1} \cdot {}^{I}I_2$
	Mode F	
11	${}^{F}C1 \Leftrightarrow {}^{F}C2$	$v_{11} = {}^{F}k_{C1,C2} \cdot {}^{F}C_1 - {}^{F}k_{C2,C1} \cdot {}^{F}C_2$
12	${}^{F}C2 \Leftrightarrow {}^{F}O$	$v_{12} = {}^{F}k_{C2,O} \cdot {}^{F}C_2 - {}^{F}k_{O,C2} \cdot {}^{F}O$
	Mode Ca	
13	${}^{Ca1}C1 \Leftrightarrow {}^{Ca1}C2$	$v_{13} = {}^{Ca1}k_{C1,C2} \cdot {}^{Ca1}C_1 - {}^{Ca1}k_{C2,C1} \cdot {}^{Ca1}C_2$
14	${}^{Ca1}C2 \Leftrightarrow {}^{Ca1}I_3$	$v_{14} = {}^{Ca1}k_{C2,O} \cdot {}^{Ca1}C_2 - {}^{Ca1}k_{O,C2} \cdot {}^{Ca1}I_3$

(continued on next page)

Table A1 (*continued*)

Number	Elementary steps	Equations for transition rates
Intramodal transitions		
	Mode Ca	
15	$^{Ca1}C1 \Leftrightarrow {}^{Ca1}I1$	$v_{15}={}^{Ca1}k_{C1,I1}\cdot{}^{Ca1}C_1-{}^{Ca1}k_{I1,C1}\cdot{}^{Ca1}I_1$
16	$^{Ca1}C2 \Leftrightarrow {}^{Ca1}I2$	$v_{16}={}^{Ca1}k_{C2,I2}\cdot{}^{Ca1}C_2-{}^{Ca1}k_{I2,C2}\cdot{}^{Ca1}I_2$
17	$^{Ca1}I1 \Leftrightarrow {}^{Ca1}I2$	$v_{17}={}^{Ca1}k_{I1,I2}\cdot{}^{Ca1}I_1-{}^{Ca1}k_{I2,I1}\cdot{}^{Ca1}I_2$
18	$^{Ca2}C1 \Leftrightarrow {}^{Ca2}C2$	$v_{18}={}^{Ca2}k_{C1,C2}\cdot{}^{Ca2}C_1-{}^{Ca2}k_{C2,C1}\cdot{}^{Ca2}C_2$
19	$^{Ca2}C2V^{Ca2}I_3$	$v_{19}={}^{Ca2}k_{C2,O}\cdot{}^{Ca2}C_2-{}^{Ca2}k_{O,C2}\cdot{}^{Ca2}I_3$
20	$^{Ca2}C1V^{Ca2}I1$	$v_{20}={}^{Ca2}k_{C1,I1}\cdot{}^{Ca2}C_1-{}^{Ca2}k_{I1,C1}\cdot{}^{Ca2}I_1$
21	$^{Ca2}C2 \Leftrightarrow {}^{Ca2}I2$	$v_{21}={}^{Ca2}k_{C2,I2}\cdot{}^{Ca2}C_2-{}^{Ca2}k_{I2,C2}\cdot{}^{Ca2}I_2$
22	$^{Ca2}I1 \Leftrightarrow {}^{Ca2}I2$	$v_{22}={}^{Ca2}k_{I1,I2}\cdot{}^{Ca2}I_1-{}^{Ca2}k_{I2,I1}\cdot{}^{Ca2}I_2$
Intermodal Ca^{2+}-dependent transitions		
23	$^{B}C_1+Ca_{sm} \Leftrightarrow {}^{I}C_1$	$v_{23}={}^{C1}l_{B,I}\cdot{}^{B}C_1\cdot Ca_{sm}-{}^{C1}l_{I,B}\cdot{}^{I}C_1$
24	$^{B}C_2+Ca_{sm} \Leftrightarrow {}^{I}C_2$	$v_{24}={}^{C2}l_{B,I}\cdot{}^{B}C_2\cdot Ca_{sm}-{}^{C2}l_{I,B}\cdot{}^{I}C_2$
25	$^{B}O+Ca_{sch} \Leftrightarrow {}^{I}I_3$	$v_{25}={}^{O}l_{B,I}\cdot{}^{B}O\cdot Ca_{sch}-{}^{O}l_{I,B}\cdot{}^{I}I_3$
26	$^{I}C_1+Ca_{sm} \Leftrightarrow {}^{Ca1}C_1$	$v_{26}={}^{C1}l_{I,Ca1}\cdot{}^{I}C_1\cdot Ca_{sm}-{}^{C1}l_{Ca1,I}\cdot{}^{Ca1}C_1$
27	$^{I}C_2+Ca_{sm} \Leftrightarrow {}^{Ca1}C_2$	$v_{27}={}^{C2}l_{I,Ca1}\cdot{}^{I}C_2\cdot Ca_{sm}-{}^{C2}l_{Ca1,I}\cdot{}^{Ca1}C_2$
28	$^{I}I_3+Ca_{sm} \Leftrightarrow {}^{Ca1}I_3$	$v_{28}={}^{I3}l_{I,Ca1}\cdot{}^{I}I_3\cdot Ca_{sm}-{}^{I3}l_{Ca1,I}\cdot{}^{Ca1}I_3$
Ca^{2+}-independent intermodal transitions		
29	$^{I}C_1 \Leftrightarrow {}^{F}C_1$	$v_{29}={}^{C1}l_{I,F}\cdot{}^{I}C_1-{}^{C1}l_{F,I}\cdot{}^{F}C_1$
30	$^{I}C_2 \Leftrightarrow {}^{F}C_2$	$v_{30}={}^{C2}l_{I,F}\cdot{}^{I}C_2-{}^{C2}l_{F,I}\cdot{}^{F}C_2$
31	$^{I}I_3 \Leftrightarrow {}^{F}O$	$v_{31}={}^{O}l_{I,F}\cdot{}^{I}I_3-{}^{O}l_{F,I}\cdot{}^{F}O$
32	$^{Ca1}C_1 \Leftrightarrow {}^{Ca2}C_1$	$v_{32}={}^{C1}l_{Ca1,Ca2}\cdot{}^{Ca1}C_1-{}^{C1}l_{Ca2,Ca1}\cdot{}^{Ca2}C_1$
33	$^{Ca1}C_2 \Leftrightarrow {}^{Ca2}C_2$	$v_{33}={}^{C2}l_{Ca1,Ca2}\cdot{}^{Ca1}C_2-{}^{C2}l_{Ca22,Ca1}\cdot{}^{Ca2}C_2$
34	$^{Ca1}I_3 \Leftrightarrow {}^{Ca2}I_3$	$v_{34}={}^{O}l_{Ca1,Ca2}\cdot{}^{Ca1}O-{}^{O}l_{Ca22,Ca1}\cdot{}^{Ca2}O$

Here, the rate constants for intramodal switches within mode X (X=B, I, F, Ca1, Ca2) are designated by symbols ${}^{X}k$ and the rate constants for intermodal switches are designated by ${}^{Y}l$, where Y=C_1, C_2, O, I_3. The model assumes that ${}^{B}k_{C2,O}={}^{I}k_{C2,O}$, ${}^{B}k_{O,C2}={}^{I}k_{O,C2}$, ${}^{C1}l_{I,F}={}^{C2}l_{I,F}$, ${}^{C1}l_{F,I}={}^{C2}l_{F,I}$, ${}^{B}\alpha_1={}^{I}\alpha_1={}^{F}\alpha_1={}^{Ca}\alpha_1$, ${}^{B}\alpha_2={}^{I}\alpha_2={}^{F}\alpha_2={}^{Ca}\alpha_2$.

For simplicity, it is assumed that intermodal transitions of inactivated states (I_1 and I_2) are very slow, and they are not considered in this work. In addition, limitations are imposed on other rate constants for transitions representing closed cycles:

$${}^{F}k_{C_2,O}{}^{*C_1}l_{I,F}{}^{*O}l_{F,I}{}^{*I}k_{I,C_2}{}^{*F}k_{O,C_2}{}^{*C1}l_{F,I}{}^{*O}l_{I,F}{}^{*I}k_{C_2,I}$$

$${}^{X}k_{C_2I_2}{}^{*X}k_{I_1,C_1}{}^{*}\exp\left(\frac{V_2-V_1}{K}\right)={}^{X}k_{I_2,C_2}{}^{*X}k_{C_1,I_1},$$

where $X = B, I, Ca_1, Ca_2$.

Appendix B

Differential equations describing intra- and intermodal transitions in L-type Ca^{2+} channels:

$$\frac{d({}^{B}C_1)}{dt} = -V_1 - V_3 - V_{23}$$

$$\frac{d({}^{B}C_2)}{dt} = -V_1 - V_2 - V_4 - V_{24}$$

$$\frac{d({}^{B}I_1)}{dt} = V_3 - V_5$$

$$\frac{d({}^{B}I_2)}{dt} = V_4 - V_5$$

$$\frac{d({}^{B}O)}{dt} = V_2 - V_{25}$$

$$\frac{d({}^{I}C_1)}{dt} = -V_6 - V_8 - V_{26} - V_{29}$$

$$\frac{d({}^{I}C_2)}{dt} = V_6 - V_7 - V_9 - V_{27} - V_{30}$$

$$\frac{d({}^{I}I_1)}{dt} = V_8 - V_{10}$$

$$\frac{d({}^{I}I_2)}{dt} = V_9 - V_{10}$$

$$\frac{d({}^{I}I_3)}{dt} = V_7 - V_{28} - V_{31}$$

$$\frac{d({}^{F}C_1)}{dt} = V_{29} - V_{11}$$

$$\frac{d({}^{C}C_2)}{dt} = V_{11} - V_{12} + V_{30}$$

$$\frac{d({}^{F}O)}{dt} = V_{12} + V_{31}$$

$$\frac{d({}^{Ca_1}C_1)}{dt} = V_{26} - V_{13} - V_{15} - V_{32}$$

$$\frac{d({}^{Ca_1}C_2)}{dt} = V_{27} - V_{13} - V_{14} - V_{16} - V_{33}$$

$$\frac{d({}^{Ca_1}I_1)}{dt} = V_{15} - V_{17}$$

$$\frac{d({}^{Ca_1}I_2)}{dt} = V_{16} + V_{17}$$

$$\frac{d({}^{Ca_1}I_3)}{dt} = V_{28} + V_{14} - V_{34}$$

$$\frac{d({}^{Ca_2}C_1)}{dt} = V_{32} - V_{18} - V_{20}$$

$$\frac{d({}^{Ca2}C_2)}{dt} = V_{33} + V_{18} - V_{19} - V_{21}$$

$$\frac{d({}^{Ca_2}I_1)}{dt} = V_{20} - V_{22}$$

$$\frac{\mathrm{d}\left({}^{Ca2}\mathrm{I}_2\right)}{\mathrm{d}t} = V_{21} + V_{22}$$

$$\frac{\mathrm{d}\left({}^{\mathrm{Ca2}}\mathrm{I}_3\right)}{\mathrm{d}t} = V_{34} + V_{19}$$

$$\frac{\mathrm{d}(\mathrm{Ca}_{\mathrm{sm}})}{\mathrm{d}t} = \frac{\left(-\frac{\sigma\lambda ip_0}{2FD} + \mathrm{Ca}_{\mathrm{in}} - \mathrm{Ca}_{\mathrm{sm}}\right)D}{\lambda^2}, \tag{B1}$$

where open probability $\boldsymbol{p}_0 = {}^{\mathrm{B}}\mathrm{O} + {}^{\mathrm{F}}\mathrm{O}$.

Single ($\boldsymbol{i}$) and integral ($\boldsymbol{I}_{\mathrm{Ca}}$) Ca^{2+} currents in whole-cell voltage-clamp experiments [21] were described as follows:

$$i = P_{\mathrm{Ca}}F\left(\frac{F}{RT}\right)2V\frac{\mathrm{Ca}_{\mathrm{out}}\exp\left(-\frac{2VF}{RT}\right) - \mathrm{Ca}_{\mathrm{in}}}{\exp\left(-\frac{2VF}{RT}\right) - 1} \tag{B2}$$

$$I_{\mathrm{Ca}} = i\sigma Sp_0, \tag{B3}$$

where $\boldsymbol{S}$ is the area of the entire membrane.

Single channel Ca^{2+} currents in whole-cell configuration of voltage-clamp experiments [66] was described by the following linear function:

$$i = 10^{-3}g_{\mathrm{Ca}}(V - 37), \tag{B4}$$

where 10^{-3} is the normalizing factor, which was introduced to bring the units of measurement into correspondence.

All variables and parameters are explained in the main text.

References

[1] T.F. McDonald, S. Pelzer, W. Trautwein, D. Pelzer, Regulation and modulation of calcium channels in cardiac, skeletal, and smooth muscle cells, Physiol. Rev. 74 (1994) 365–507.

[2] W.A. Catterall, Structure and regulation of voltage-gated Ca^{2+} channels, Annu. Rev. Cell. Dev. Biol. 16 (2000) 521–555.

[3] R. Eckert, J.E. Chad, Inactivation of Ca channels, Prog. Biophys. Mol. Biol. 44 (1984) 215–267.

[4] T.W. Soong, A. Stea, C.D. Hodson, S.J. Dubel, S.R. Vincent, T.P. Snutch, Structure and functional expression of a member of the low voltage-activated calcium channel family, Science 260 (1993) 1133–1136.

[5] M. De Leon, Y. Wang, L. Jones, E. Perez-Reyes, X. Wei, T.W. Soong, T.P. Snutch, D.T. Yue, Essential Ca^{2+}-binding motif for Ca^{2+}-sensitive inactivation of L-Type Ca^{2+} channels, Science 270 (1995) 1502–1506.

[6] B.Z. Peterson, C.D. DeMaria, J.P. Adelman, D.T. Yue, Calmodulin is the sensor for Ca^{2+}-dependent inactivation of L-Type Ca^{2+} channels, Neuron 22 (1999) 549–558.

[7] N.M. Soldatov, R.D. Zuhlke, A. Bouron, H. Reuter, Molecular structures involved in L-type calcium channel inactivation. Role of the carboxyl-terminal region encoded by exons 40–42 in alpha1C subunit in the kinetics and Ca2+ dependence of inactivation, J. Biol. Chem. 272 (1997) 3560–3566.

[8] N.M. Soldatov, M. Oz, K.A. O'Brien, D.R. Abernethy, M. Morad, Molecular determinants of L-type Ca2+ channel inactivation. Segment exchange analysis of the carboxyl-terminal cytoplasmic motif encoded by exons 40–42 of the human alpha1C subunit gene, J. Biol. Chem. 273 (1998) 957–963.

[9] R.D. Zhulke, H. Reuter, Ca^{2+}-sensitive inactivation of L-type Ca^{2+} channels depends on multiple cytoplasmic amino acid sequences of the α_{1C} subunit, Proc. Natl. Acad. Sci. USA 95 (1998) 3287–3294.

[10] N. Qin, R. Olcese, M. Bransby, T. Lin, L. Birnbaumer, Ca2+-induced inhibition of the cardiac Ca^{2+} channel depends on calmodulin, Proc. Natl. Acad. Sci. USA 96 (1999) 2435–2438.

[11] B.Z. Peterson, J.S. Lee, J.G. Mulle, Y. Wang, M. Leon, D.T. Yue, Critical Determinants of Ca^{2+}-Dependent Inactivation within an EF-Hand Motif of L-Type Ca^{2+} Channels, Biophys. J. 78 (2000) 1906–1920.

[12] C. Romanin, R. Gamsjaeger, H. Kahr, D. Schaufler, O. Carlson, D. Abernethy, N. Soldatov, Ca^{2+} sensors of L-type Ca^{2+} channel, FEBS Letters 487 (2000) 301–306.

[13] G.S. Pitt, R.D. Zuhlke, A. Hudmon, H. Schulman, H. Reuter, R.W. Tsien, Molecular basis of calmodulin tethering and Ca^{2+}-dependent inactivation of L-type Ca^{2+} channels, J. Biol. Chem. 276 (2001) 30794–30802.

[14] M.G. Erickson, H. Liang, M.X. Mori, D.T. Yue, FRET two-hybrid mapping reveals function and location of L-type Ca^{2+} channel CaM preassociation, Neuron 39 (2003) 97–107.

[15] J. Kim, S. Ghosh, D.A. Nunziato, G.S. Pitt, Identification of the components controlling inactivation of voltage-gated Ca^{2+} channels, Neuron 41 (2004) 745–754.

[16] R.D. Zuhlke, G.S. Pitt, K. Deisseroth, R.W. Tsien, H. Reuter, Calmodulin supports both inactivation and facilitation of L-type Ca^{2+} channels, Nature 399 (1999) 159–162.

[17] J. Mouton, A. Fetz, Y. Maulet, Interactions of calmodulin with two peptides derived from the C-terminal cytoplasmic domain of the $Ca_V1.2$ Ca^{2+} channel provide evidence for a molecular switch involved in Ca^{2+}-induced inactivation, J. Biol. Chem. 276 (2001) 22359–22367.

[18] N.M. Soldatov, Ca^{2+} channel moving tail: link between Ca^{2+}-induced inactivation and Ca^{2+} signal transduction, Trends Pharmacol. Sci. 24 (2003) 167–171.

[19] L. Sun, J.-S. Fan, J.W. Clark, P.T. Palade, A model of the L-type Ca^{2+} channel in rat ventricular myocytes: ion selectivity and inactivation mechanism, J. Physiol. 529 (2000) 139–158.

[20] C.D. DeMaria, T.W. Soong, B.A. Alseikhan, R.S. Alvania, D.T. Yue, Calmodulin bifurcates the local Ca^{2+} signal that modulates P/Q-type Ca^{2+} channels, Nature 411 (2001) 484–489.

[21] J. Chad, R. Eckert, D. Ewald, Kinetics of calcium-dependent inactivation of calcium current in voltage-clamped neurones of *Aplysia californica*, J. Physiol. 347 (1984) 279–300.

[22] A. Sherman, J. Keizer, J. Rinzel, Domain model for Ca^{2+}-inactivation of Ca^{2+} channels at low channel density, Biophys. J. 58 (1990) 985–995.

[23] A.R. Kay, Inactivation kinetics of calcium current of acutely dissociated CA1 pyramidal cells of the mature guinea-pig hippocampus, J. Physiol. 437 (1991) 27–48.

[24] R.W. Hadley, W.J. Lederer, Ca^{2+} and voltage inactivate Ca^{2+} channels in guinea-pig ventricular myocytes through independent mechanisms, J. Physiol. 444 (1991a) 257–268.

[25] R. Shirokov, R. Levis, N. Shirokova, E. Rios, Two classes of gating current from L-type Ca channels in guinea pig ventricular myocytes, J. Gen. Physiol. 99 (1992) 863–895.

[26] R. Shirokov, R. Levis, N. Shirokova, E. Rios, Ca^{2+}-dependent inactivation of cardiac L-tipe Ca^{2+} channels does not affect their voltage sensor, J. Gen. Physiol. 102 (1993) 1005–1030.

[27] J.P. Imredy, D.T. Yue, Submicroscopic Ca^{2+} diffusion mediates inhibitory coupling between individual Ca^{2+} channels, Neuron 9 (1992) 197–207.

[28] G.F. Hofer, K. Hohenthanner, W. Baumgarther, K. Groscher, N. Klugbauer, F. Hofmann, C. Romanin, Intracellular Ca^{2+} inactivates L-type Ca^{2+} channels with a Hill coefficient of ~1 and an inhibition

constant of ~4 μM by reducing cannel's open probability, Biophys. J. 73 (1997) 1857–1865.
[29] F. Bezanilla, The voltage sensor in voltage-dependent ion channels, Physiol. Rev. 80 (2000) 555–592.
[30] F. Bezanilla, Voltage sensor movements, J. Gen. Physiol. 120 (2002) 465–473.
[31] A. Cavalie', R. Ochi, D. Pelzer, W. Trautwein, Elementary currents through Ca^{2+} channels in Guinea pig myocytes, Pflügers Arch. 398 (1983) 284–297.
[32] A. Cavalie', D. Pelzer, W. Trautwein, Fast and slow gating behaviour of single calcium channels in cardiac cells. Relation to activation and inactivation of calcium-channel current, Pflügers Arch. 406 (1986) 241–258.
[33] A.M. Brown, H.D. Lux, D.L. Wilson, Activation and inactivation of single channels in snail neurons, J. Gen. Physiol. 83 (1984) 751–769.
[34] R. Shirokov, G. Ferreira, J. Yi, E. Rios, Inactivation of gating currents of L-type calcium channels, J. Gen. Physiol. 111 (1998) 807–823.
[35] T. Hoshi, S.J. Smith, Large depolarization induces long opening of voltage-dependent calcium channels in adrenal chromaffin cells, J. Neurosci. 7 (1987) 571–580.
[36] R.W. Hadley, W.J. Lederer, Properties of L-type calcium channel gating current in isolated guinea pig ventricular myocytes, J. Gen. Physiol. 98 (1991b) 265–285.
[37] M. Mazzanti, L.J. DeFelice, Y.M. Liu, Gating of L-type Ca^{2+} channels in embrionic chock ventricle cells: Dependence on voltage, current and channel density, J. Physiol. 443 (1991) 307–334.
[38] R.W. Hadley, W.J. Lederer, Properties of L-type calcium channel gating current in isolated guinea pig ventricular myocytes, J. Gen. Physiol. 98 (1991b) 265–285.
[39] S. Hering, S. Berjukow, S. Sokolov, R. Marksteiner, R.G. Weib, R. Kraus, E.N. Timin, Molecular determinants of inactivation in voltage-gated Ca^{2+} channels, J. Physiol. 528.2 (2000) 237–249.
[40] S.C. Stotz, J. Hamid, R.L. Spaetgens, S.E. Jarvis, G.W. Zamponi, Fast inactivation of voltage-dependent calcium channels, J. Biol. Chem. 275 (2000) 24575–24582.
[41] I. Findlay, Physiological modulation of inactivation in L-type Ca^{2+} channels: One switch, J. Physiol. 554 (2004) 275–283.
[42] C. Shi, N.M. Soldatov, Molecular determinants of voltage-dependent slow inactivation of the Ca^{2+} channel, J. Biol. Chem. 277 (2002) 6813–6821.
[43] G. Ferreira, E. Rios, N. Reyes, Two components of voltage-dependent inactivation in $Ca_V1.2$ channels revealed by its gating currents, Biophys. J. 84 (2003) 3662–3678.
[44] T. Cens, S. Restituito, S. Galas, P. Charnet, Voltage and calcium use the same molecular determinants to inactivate calcium channels, J. Biol. Chem. 274 (1999) 5483–5490.
[45] C. Chen, P. Hess, Mechanism of gating of T-type calcium channels, J. Gen. Physiol. 96 (1990) 603–630.
[46] H.D. Lux, A.M. Brown, Single channel studies on inactivation of calcium currents, Science 225 (1984) 432–434.
[47] M.J. Gutnick, H.D. Lux, D. Swandulla, H. Zuker, Voltage-dependent and calcium-dependent inactivation of calcium channel current in identified snail neurons, J. Physiol. 412 (1989) 197–220.
[48] G. Isenberg, U. Klöckner, Calcium currents of isolated bovine ventricular myocytes are fast and large amplitude, Pflügers Arch. 395 (1982) 30–41.
[49] D.L. Campbell, W.R. Giles, J.R. Hume, E.F. Shibata, Inactivation of calcium current in bull-frog atrial myocytes, J. Physiol. 403 (1988) 287–315.
[50] T.D. Plant, Properties and calcium-dependent inactivation of calcium currents in cultured mouse pancreatic B-cells, J. Physiol. 404 (1988) 731–747.
[51] R.G. Miller, Voltage-sensitive Ca^{2+} channels, J. Biol. Chem. 267 (1992) 1403–1406.
[52] M. Villain, P. Jackson, W.J. Doong, D. Muccio, J.E. Blalock, Characterization of an atypical Ca^{2+} binding motif from L-type Ca^{2+} channels, Biophys. J. 76 (1999) 101a (Abstr.).
[53] J. Zhou, R. Olcese, N. Qin, F. Noceti, L. Birnbaumer, E. Stefani, Feedback inhibition of Ca2+ channels by Ca2+ depends on a short sequence of the C terminus that does not include the Ca2+ -binding function of a motif with similarity to Ca2+ -binding domains, Proc. Natl. Acad. Sci. U. S. A. 94 (1997) 2301–2305.
[54] G. Bernatchez, D. Talwar, L. Parent, Mutations in the EF-hand motif impair the inactivation of barium currents of the cardiac α_{1C} channel, Biophys. J. 75 (1998) 1727–1739.
[55] J.J. Falke, S.K. Drake, A.L. Hazard, O.B. Peersen, Molecular tuning of ion binding to calcium signaling proteins, Q. Rev. Biophys. 27 (1994) 219–290.
[56] R.D. Zuhlke, G.S. Pitt, R.W. Tsien, H. Reuter, Ca2+-sensitive inactivation and facilitation of L-type Ca2+ channels both depend on specific amino acid residues in a consensus calmodulin-binding motif in the (alpha)1C subunit, J. Biol. Chem. 275 (2000) 21121–22129.
[57] J. Chad, R. Eckert, Calcium domains associated with individual channels can account for anomalous voltage relations of Ca-dependent responses, Biophys. J. 45 (1984) 993–999.
[58] S.M. Simon, R.R. Llina's, Compartmentalization of the submembrane calcium activity during calcium influx and its significance in transmitter release, Biophys. J. 48 (1985) 485–498.
[59] R. Llinas, M. Sugimori, R.B. Silver, Microdomain of high calcium concentration in presinaptical terminal, Science 256 (1992) 677–679.
[60] E. Neher, Concentration profiles of intracellular calcium in the presence of a diffusible chelator, Exp. Brain Res. Ser. 14 (1986) 80–96.
[61] M.D. Stern, Buffering of calcium in the vicinity of a channel pore, Cell Calcium 13 (1992) 183–192.
[62] A.L. Hodgkin, B. Katz, The effect of calcium on the axoplasm of giant nerve fibers, J. Exp. Biol. 26 (1949) 292–294.
[63] J.P. Imredy, D.T. Yue, Submicroscopic Ca^{2+} diffusion mediates inhibitory coupling between individual Ca^{2+} channels, Neuron 9 (1992) 197–207.
[64] Y. Takagishi, S. Rothery, J. Issberner, A. Levi, N.J. Severs, Spatial distribution of dihydropyridine receptors in the plasma membrane of guinea pig cardiac myocytes investigated by correlative confocal microscopy and label-fracture electron microscopy, J. Electron. Microsc. (Tokyo) 46 (1997) 165–170.
[65] I. Goryanin, T.C. Hodgman, E. Selkov, Mathematical simulation and analysis of cellular metabolism and regulation, Bioinformatics 15 (1999) 749–758.
[66] W.C. Rose, C.W. Balke, W.G. Wier, E. Marban, Macroscopic and unitary properties of physiological ion flux through L-type Ca^{2+} channels in guinea-pig heart cells, J. Physiol. 456 (1992) 267–284.
[67] D.W. Marquardt, An algorithm for least-squares estimation of nonlinear parameters, J. SIAM 11 (1963) 431–441.
[68] Y. You, D.J. Pelzer, S. Pelzer, Modulation of L-type Ca^{2+} current by fast and slow Ca^{2+} buffering in guinea pig ventricular cardiomyocytes, Biophys. J. 72 (1997) 175–187.
[69] J.A. Haack, R.L. Rosenberg, Calcium-dependent inactivation of L-type calcium channels in planar lipid bilayers, Biophys. J. 66 (1994) 1051–1060.
[70] J.A. Argibay, R. Fishmeister, H.C. Hartzell, Inactivation, reactivation, and pacing dependence of calcium current in frog cardiocytes: Correlation with current density, J. Physiol. 401 (1988) 201–226.